

# Fast Emulation and Modular Calibration for Simulators with Functional Response

Grant Hutchings\*

Department of Statistics, Simon Fraser University  
and

Derek Bingham

Department of Statistics, Simon Fraser University  
and

Earl Lawrence

Department of Statistics, Los Alamos National Laboratory

May 28, 2024

## Abstract

Scalable surrogate models enable efficient emulation of computer models (or simulators), particularly when dealing with large ensembles of runs. While Gaussian Process (GP) models are commonly employed for emulation, they face limitations in scaling to truly large datasets. Furthermore, when dealing with dense functional output, such as spatial or time-series data, additional complexities arise, requiring careful handling to ensure fast emulation. This work presents a highly scalable emulator for functional data, building upon the works of Kennedy and O’Hagan (2001) and Higdon et al. (2008), while incorporating the local approximate Gaussian Process framework proposed by Gramacy and Apley (2015). The emulator utilizes global GP lengthscale parameter estimates to scale the input space, leading to a substantial improvement in prediction speed. We demonstrate that our fast approximation-based emulator can serve as a viable alternative to the methods outlined in Higdon et al. (2008) for functional response, while drastically reducing computational costs. The proposed emulator is applied to quickly calibrate the multiphysics continuum hydrodynamics simulator FLAG with a large ensemble of 20000 runs. The methods presented are implemented in the R package **FlaGP**.

*Keywords:* Scalable Gaussian Process, local approximate Gaussian Process (laGP), Computer Experiments, Empirical Orthogonal Functions (EOF), Surrogate Model

---

\*The authors gratefully acknowledge *Simon Fraser University* and *Los Alamos National Laboratory*.

# 1 Introduction

Computer models (or simulators) have become fundamental in the study of complex physical systems. In some cases, the computer models are so computationally intensive that only a small number of runs are performed at different input settings (Sacks et al., 1989), while in other cases, the simulator may be very fast to evaluate and a large ensemble of trials can be conducted (e.g. Francom et al. (2019), Kaufman et al. (2011), etc.). Even with computational advancements resulting in larger simulation designs, computer models are often too time consuming to run in real time. Statistical surrogate models, or emulators, remain a key tool enabling fast exploration of the simulator response. In this paper, the principal motivation is very fast emulation and uncertainty quantification (UQ) for simulators with functional outputs and large ensembles of model evaluations. In fact, for the applications we are interested in, the computer model is to be deployed in experimental facilities and should provide results in close to real time.

Gaussian Process models (GP's) have been the gold standard for computer model emulation (Sacks et al., 1989). They are flexible predictors that provide a foundation for uncertainty in deterministic settings. GP models are, however, limited in their applicability to large ensembles due to the computational bottleneck of covariance matrix inversion. More computationally feasible forms of GP's for large datasets have been proposed in recent literature (e.g., see Katzfuss et al. (2022) and references therein). Functional data of dimension  $d_y$  adds another layer of complexity. One approach to dealing with functional response is to use the indices where the data is observed as additional inputs to the emulator such as in spatial modeling. For an ensemble of size  $M$ , the result is  $Md_y$  scalar response values. Even for relatively small ensembles, this approach is infeasible if  $d_y$  is large.

An orthogonal basis decomposition has proved to be a successful alternative as complex and non-linear functional response can often be well represented with  $p \ll d_y$  basis functions, reducing the number of response values to  $Mp$ . Higdon et al. (2008) use this idea to extend the the work of Kennedy and O'Hagan (2001) for functional response. Independent GP models are fit to empirical orthogonal functions (EOF) computed via the

Singular Value Decomposition (SVD). Their methodology has been used successfully in many applications (e.g., Walters et al. (2018)) but it does not scale to large ensembles. We will refer to the model proposed in Higdon et al. (2008) as SVDGP.

In this work, a method is proposed which makes use of the same EOF decomposition, but uses a local approximate GP (laGP) (Gramacy and Apley, 2015) (implemented in the R package `laGP` (Gramacy, 2016)), which leverages local designs to reduce the size of the covariance matrix, resulting in significant computational savings.

There are other works applying GP models to large functional datasets. Zhang et al. (2018) are also motivated by laGP, and built prediction neighborhoods using an optimality criterion. Zhang et al. (2018) and Gramacy (2016) show that the cost of computing optimal prediction neighborhoods is significant. As a result, their methods cannot achieve the speed desired for our applications. This is made clear in the supplementary material, for example; A simulation study is presented showing that for random data of size  $M = 20000$ , representing the application dataset in this work, the default laGP neighborhood selection criterion is approximately 4 times slower than nearest neighbors (NN). While it is well known that NN's are suboptimal for prediction (Vecchia (1988), Stein et al. (2004)), the proposed method uses input scaling (Hsu (2019), Sun et al. (2019)) to dramatically improve NN prediction. Section 3.1 provides a detailed discussion of input scaling and its effect on NN prediction.

Ma et al. (2022) are also motivated by the emulation of a computer model with functional output. Rather than the SVD, an active subspace approach is used to determine basis functions (Constantine et al., 2014), and a Bayesian approach to emulation is taken with the nearest-neighbor GP (NNGP) model (Datta et al., 2016). The NNGP model is based on the Vecchia approximation (Vecchia, 1988). Katzfuss et al. (2022) use the Vecchia approximation with fisher scoring (and input scaling) for fast GP inference and prediction with large datasets. Importantly, the Vecchia approximation has significant overhead in selecting conditioning sets, which the proposed emulator avoids. The supplementary material contains an illustration of this.

An important use of emulators is model calibration. Conventionally, computer model

calibration follows the methods in Kennedy and O’Hagan (2001), and Higdon et al. (2008) extend this methodology for functional responses. Neither Zhang et al. (2018), Ma et al. (2022), or Katzfuss et al. (2022) apply their methods to calibration problems, a key motivation for this work. The proposed method takes a modular (Bayarri et al., 2009) approach to calibration, where the emulator is fit using only the computer model output. Section 4 discusses the benefits of modular calibration for the problems that motivated this work.

Modularization, local prediction, and input scaling are all ways in which a large degree of scalability is achieved. Gramacy et al. (2015) also use these ideas for emulation and calibration of simulators with scalar response. The calibration framework proposed here extends their work in two ways; first is the extension to functional response, and second is the use of MCMC for posterior inference on calibration parameters. In Section 3.1 we will discuss how input scaling is key for fast calibration with MCMC. Our methods are developed around MCMC because uncertainty in the calibration parameters is usually desired. For some applications a faster maximum a-posteriori (MAP) estimate of calibration parameters is sufficient, such as multistage modeling where a only a point estimate of parameters is propagated forward to another model. A MAP approach is developed for the proposed model in Section 4.3.

We note that other scalable GP frameworks could potentially be adopted for the task of fast emulation and modular calibration. Compactly supported covariance functions provide a means of scaling GP models to large datasets by leveraging sparse matrix computations. We chose not to pursue such models because Hsu (2019) present a comparison of laGP and the sparse covariance GP model in Kaufman et al. (2011). They find that laGP provides superior prediction in less time on a range of datasets. Maximum Likelihood inference for GP parameters has also been used to speed up the Bayesian SVDGP model (Chang et al., 2014). Regardless of the inference method, GP models that do not leverage sparsity in any way remain limited by  $\mathcal{O}(M^3)$  scaling, so they are infeasible for our large application dataset.

This paper is structured as follows; In Section 2 the motivating application and dataset are described. Section 3 describes the SVDGP model, highlighting limitations for large

datasets. The proposed emulation method is then described in detail, focusing on alleviating the computational bottlenecks of GP modeling and prediction with laGP. In Section 3.2, a working example is presented to illustrate the method with a comparison to SVDGP. Section 4 shows how the fast emulator is used for modular calibration with a similar working example. A fast point estimation procedure for the calibration parameters is developed in 4.3. Section 5 presents an analysis of the motivating dataset. In Section 6 there is a discussion of the results, highlighting the strengths and weaknesses of the proposed method, which is hereby referred to as FlaGP.

## 2 Application

The proposed methodology is demonstrated on the multiphysics continuum hydrodynamics code FLAG (Burton, 2007), a deterministic computer model for high strain-rate and deformation responses for materials science. A large ensemble of  $M = 20000$  runs from FLAG is available for analysis, simulating an Aluminum sample impacted by an Aluminum flyer plate over a range of experimental conditions. The ensembles span an 11-dimensional input space. Inputs include those for the Johnson-Cook strength model (Johnson and Cook, 1983) ( $A, B, C, n_{JC}, m_{JC}$ ), the flyer impact velocity ( $v_1, v_2, v_3$ ), and the material shear modulus ( $G_1, \Delta_2, \Delta_3$ ). Simulator outputs are available for 3 “shots” associated with varied flyer plate and sample thickness; referred to as shots *104*, *105*, and *106*. Each velocity and shear modulus parameter is associated with a single shot.

The output of these simulations are 1-d profiles of the impacted sample free surface velocity over time. In addition to the computer model output, data is available from a single field experiment for each of the shots (Boteler and Dandekar, 2006). This work explores emulating FLAG as well as using the experiment to calibrate these 11 parameters. Fig. 1 shows the 3 experimental shots in the left panel, and on the right, shot *105*, along with a subset of the simulations.

A smaller ensemble of 1000 runs from FLAG, simulating the same experiments, was analyzed using the SVDGP model at great computational expense (Walters et al., 2018). In their work, only 4 features along each curve were extracted for emulation and calibration.

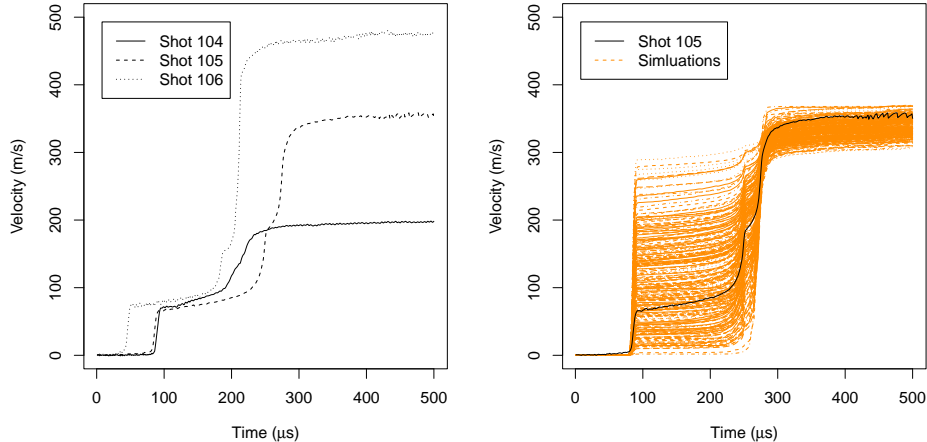


Figure 1: Left: Velocity profiles for 3 observed shots. Right: Shot *105* and a subset of the FLAG simulations.

Using a Python implementation of the SVDGP model in the **SEPIA** package (Gattiker et al., 2020), we estimate that their calibration took up to 10 days of computing time. The supplementary material contains a comparison to their analysis using FlaGP and we find that competitive emulation and calibrated predictions can be achieved in a fraction of the time. Section 5 presents a significantly more computationally tractable analysis for the large ensemble and uses the entire velocity curve sampled at 500 time points for emulation and calibration. The aim is to deploy the emulator in an experimental facility where calibration can be done very quickly, enabling rapid updating with new experimental data.

### 3 Emulator Formulation

The common approach to computer model emulation for functional outputs is outlined here. In doing so, notation is introduced, and challenges with large datasets highlighted.

Let  $\mathbf{z}(\mathbf{x})$  be the standardized computer model output at input  $\mathbf{x} \in \mathbb{R}^{d_x}$ , and let  $\mathbf{X}$  denote the  $M \times d_x$  ensemble design matrix, which we assume is scaled to the unit hypercube. Typically, outputs are standardized so that the mean response value for each functional index is zero, and the total variance for all the computer model outputs is 1. Let the matrix of standardized outputs be denoted by  $\mathbf{Z}(\mathbf{X}) \in \mathbb{R}^{M \times d_y}$ .

In Higdon et al. (2008), an orthogonal basis emulator for the computer model output is introduced. The approach begins by computing the SVD of the standardized output matrix  $\mathbf{Z}(\mathbf{X}) = \mathbf{U}\mathbf{D}\mathbf{V}^T$ . The SVD is used to build the basis representation  $\mathbf{Z}(\mathbf{X}) = \mathbf{B}\mathbf{W}(\mathbf{X})$ , where  $\mathbf{B} = \mathbf{U}\mathbf{D}/\sqrt{M}$  is the matrix of basis vectors, and  $\mathbf{W}(\mathbf{X}) = \sqrt{M}\mathbf{V}^T$  are the associated weights. In practice  $p_\eta \leq \min(d_y, M)$  basis vectors are chosen so that the reconstruction error  $\mathbf{Z}(\mathbf{X}) - \mathbf{B}\mathbf{W}(\mathbf{X})$  is sufficiently small. The emulation problem is reduced to  $p_\eta$  independent, scalar GP's, trained on the weights  $\mathbf{W}$  ( $\mathbf{w}_1, \dots, \mathbf{w}_{p_\eta} \in \mathbb{R}^M$ ). The emulator has the form

$$\boldsymbol{\eta}(\mathbf{x}) = \sum_{j=1}^{p_\eta} \mathbf{b}_j w_j(\mathbf{x}). \quad (1)$$

The approach of SVDGP is to model each weight function as an independent GP. While this makes the emulation problem more conceptually manageable, the  $p_\eta$  models are limited by  $\mathcal{O}(M^3)$  scaling, making the approach infeasible for large ensemble applications.

### 3.1 Scalable Methodology

A new approach for functional emulation based on laGP is proposed that incorporates additional computational strategies to allow scalability to truly large datasets. LaGP allows for fast GP prediction using a small local subset of the data of size  $m \ll M$ . For prediction at input  $\mathbf{x}$ , a prediction neighborhood around  $\mathbf{x}$  is built using a greedy algorithm, the details of which can be found in Gramacy and Apley (2015). Importantly, the building of these subsets takes much more time than computing nearest neighbors (NN). The added computation is significant in for example a calibration setting where many thousands of predictions must be computed sequentially. Rumsey et al. (2023) also discuss the high computation cost of sequential prediction with laGP due to the building of these subsets.

It is known that NN's are suboptimal for prediction, one reason is that neighbor densities are uniform in each dimension, which is problematic when an anisotropic correlation function is used and changes in one dimension have a greater effect on predictions than another. In that case NN's will not be the points of highest correlation to the prediction location. The proposed approach uses input scaling to overcome this.

The computational benefits of laGP are clear, but it is important to note that it is a local predictor, not a global model for the data. Scalable GP frameworks such as the Vecchia approximation (Vecchia, 1988) and NNGP (Datta et al., 2016) do provide a joint distribution for the data, but at significant computational cost; the overhead associated with the data ordering and conditioning. The proposed implementation of laGP avoids this cost, providing a platform for extremely fast prediction.

Another reason the default implementation of laGP cannot provide extremely fast sequential prediction is parameter estimation. Even for small  $m$ , the cost can be prohibitive in a Bayesian calibration setting where it must be done many thousands of times. The methods described in this section yield significant computational savings by tackling both the computational bottlenecks of parameter estimation and neighborhood selection.

### 3.1.1 Lengthscale Estimation and Input Scaling

The proposed methodology uses input scaling (Hsu, 2019) to significantly reduce the computational burden of sequential prediction with laGP. An input  $\mathbf{x}$  is scaled by estimates of the global lengthscale parameters. Given estimates  $\hat{\mathbf{l}} = (\hat{l}_1, \dots, \hat{l}_{d_x})$ ,  $\mathbf{x}^{sc} = \mathbf{x} / \sqrt{\hat{\mathbf{l}}}$ .

Lengthscale estimates are obtained using the empirical Bayes approach implemented in the laGP package with a subset of  $m_{est} < M$  ensemble members. Gamma prior distributions for the lengthscales are chosen based on simulation inputs, and lengthscales are optimized using MAP estimation. As in Sun et al. (2019), bootstrapped block Latin hypercube sampling (BLHS) is used to build subsets for estimation, and the bootstrap median estimate is used which ensures consistency (Liu, 2014). For large input spaces like we have in the motivating examples ( $d_x = 11$ ), the computational effort of BLHS is impractically high. For these applications, a simple stratified random sampling approach with bootstrap replications is used.

We have found that setting  $m_{est}$  and the number of bootstrap replicates,  $r_{est}$ , as large as possible given computational constraints leads to improved estimation. While this increases the cost of precomputing, it does not effect the prediction and calibration costs of a deployed emulator. For FlaGP,  $p_\eta$  sets of lengthscales must be estimated,  $\{\hat{\mathbf{l}}_1, \dots, \hat{\mathbf{l}}_{p_\eta}\}$ , one set for each of the independent components of the model. These are used to generate scaled inputs



$\mathbf{X}_1^{sc}, \dots, \mathbf{X}_{p_\eta}^{sc}$ . Lengthscale estimation is only done once, and can be done in parallel so the increased cost for  $p_\eta$  estimations is often negligible.

Scaling inputs provides a twofold benefit in speed; First, in the scaled space, point pairs with the highest correlation correspond to nearest neighbors, which dramatically improves the quality of NN designs for prediction, which are much faster to compute than the optimal predictive neighborhoods implemented in laGP. Second, by scaling inputs the separable correlation function becomes isotropic and lengthscale parameters can be fixed at  $\mathbf{1}$  for prediction, rather than being estimated.

### 3.1.2 Prediction

Given lengthscale estimates, prediction at a new  $\mathbf{x}^*$  is made using transformed inputs  $\mathbf{x}_j^{sc*}$ ;  $j = 1, \dots, p_\eta$ . Training data consists of the  $m$  nearest neighbor inputs from  $\mathbf{X}_j^{sc}$  with their associated weights from  $\mathbf{w}_j$ . Integrating out the GP process variance under a reference priors yields a Student-t predictive distribution with

$$\begin{aligned} \text{mean } \mu_j(\mathbf{x}_j^{sc*}) &= \mathbf{c}(\mathbf{x}_j^{sc*})' \mathbf{C}(\mathbf{X}_j^{sc})^{-1} \mathbf{w}_j, \\ \text{scale } \sigma_j^2(\mathbf{x}_j^{sc*}) &= \frac{\Psi}{m} [1 - \mathbf{c}(\mathbf{x}_j^{sc*})' \mathbf{C}(\mathbf{X}_j^{sc})^{-1} \mathbf{c}(\mathbf{x}_j^{sc*})], \end{aligned} \quad (2)$$

and  $m$  degrees of freedom. The  $m$ -vector  $\mathbf{c}(\mathbf{x}_j^{sc*})$  contains correlations between nearest neighbor simulator outputs at inputs  $\mathbf{X}_j^{sc}$  and the prediction output at  $\mathbf{x}_j^{sc*}$ . The  $m \times m$  matrix  $\mathbf{C}(\mathbf{X}_j^{sc})$  is a correlation matrix with  $[\mathbf{C}]_{ll'} = C(\mathbf{x}_l^{sc}, \mathbf{x}_{l'}^{sc})$  and  $\Psi = \mathbf{w}_j^T \mathbf{C}(\mathbf{X}_j^{sc})^{-1} \mathbf{w}_j$ . The predictive mean in the functional response space is  $\boldsymbol{\mu}_z = \mathbf{B} \boldsymbol{\mu}_w$  where  $\boldsymbol{\mu}_w = [\mu_1, \dots, \mu_{p_\eta}]^T$ . Predictive samples of  $y$  are obtained by multiplying samples from the distribution defined in Eq. (2) by the basis matrix  $\mathbf{B}$ . The emulation procedure is summarized below.

While this emulator formulation is straightforward, it addresses only some of the computational challenges associated with fast computer model calibration. In Section 4 the theory required to apply this emulator in a likelihood based calibration framework is developed. To make the application of the above steps clear, the proposed emulator is illustrated with a working example and its performance is compared to SVDGP in Section 3.2.

---

**Algorithm 1** Emulator Formulation

---

- 1: *Precomputing*: With inputs  $\mathbf{X} \subseteq [0, 1]^{d_x}$ , and standardized outputs  $\mathbf{Z}$ , build  $\mathbf{B}$ ,  $\mathbf{W}(\mathbf{X})$  using the SVD of  $\mathbf{Z}$ .
  - 2: *Inference*: For  $j = 1, \dots, p_\eta$ , estimate correlation parameters  $\hat{\mathbf{l}}_j$  using the empirical Bayes procedure in 1aGP with BLHS or stratified sampling. Scale inputs  $\mathbf{X}_j^{sc} = \mathbf{X} / \sqrt{\hat{\mathbf{l}}_j}$ .
  - 3: *Prediction at  $\mathbf{x}$* : For  $j = 1, \dots, p_\eta$ , use scaled inputs  $\mathbf{x}_j^{sc} = \mathbf{x} / \sqrt{\hat{\mathbf{l}}_j}$  to build training data sets containing the  $m$  nearest input output pairs from  $\mathbf{X}_j^{sc}$ ,  $\mathbf{w}_j$ , and make predictions using equation (2).
- 

### 3.2 Working Example: Ball Drop

In this section a working example is presented which serves to explore the viability of the FlaGP emulator and allow comparison to the SVDGP model. Results for SVDGP use a Python implementation in the SEPIA package (Gattiker et al., 2020). All model fitting and prediction is done on a 2020 Apple M1 MacBook Pro, and all timing results are wall times.

The proposed method uses a series of approximations that are useful for large datasets where standard GP approaches cannot be fit in reasonable time. We therefore do not expect it to do as well in settings where SVDGP can be implemented. In this example we find that competitive and sometimes improved prediction can be achieved with FlaGP. While this behavior is not generally expected, we believe the trade-off in speed makes FlaGP desirable for large ensembles.

Consider an experiment where balls of varying radius are dropped from a tower, and time is recorded at certain vertical distances during the fall. Synthetic time-distance curves are generated from Eq. (3) where  $d$  and  $g$  are fixed inputs. Input  $d$  represents the distances where the functional response is observed, and  $g = 9.8m/s^2$  is the gravitational constant.

$$y(C, R_{ball}, g, d) = \frac{\text{acosh}(\exp\{Cd/R_{ball}\})}{\sqrt{Cg/R_{ball}}} \quad (3)$$

Inputs  $C, R_{ball}$  are the coefficient of drag and the radius of the ball. An ensemble of computer simulations is generated using an orthogonal array-based Latin hypercube design (OALHD)(Tang, 1993) of  $X = (R_{ball}, C)$  pairs in the domain  $[.025, .3] \times [.05, .15]$ , which is transformed to  $[0, 1]^2$  for modeling. For each set of inputs, the function is evaluated at

$\mathbf{d} = \{1, 2, \dots, 25\}$  meters ( $d_y = 25$ ). Fig. 2a shows  $M = 242$  evaluations over a single ensemble design as orange lines. Black dots and lines on this plot represent observed data for calibration and will be introduced in Section 4.1.1.

To account for the effect of a random ensemble on prediction, a Monte Carlo study is performed over 100 random OALHD’s. For each design the proposed emulator is fit and predictions are made on a fixed test set of 100  $(R_{ball}, C)$ -pairs on a regular grid over the same domain as the ensemble designs. Predictive metrics are averaged over the 100 test inputs, then presented as distributions over the random designs. The effect of ensemble size is explored by considering  $M \in \{98, 242, 578, 1058, 5618, 10082\}$ . Comparison to SVDGP is limited to  $M = 578$  due to the computational demands of the full GP model.

For this example, lengthscale parameters are estimated using BLHS. To control fitting time, the number of divisions used in BLHS, denoted as  $d_{est}$ , is changed based on the ensemble size. For the 6 ensemble sizes  $d_{est} = 2, 4, 8, 16, 50,$  and  $100$  respectively. For  $M \leq 1058$ ,  $r_{est} = 25$  and for  $M \in \{5618, 10082\}$ ,  $r_{est} = 1$ . The neighborhood size  $m$  is an important tuning parameter for the model as small neighborhoods will result in faster, but possibly less accurate predictions. Neighborhood size can also have important impacts on uncertainty quantification. For each  $M$  we explore a number of neighborhood sizes and recommend that a practitioner do the same. Predictions are made by taking 100 samples from the predictive distributions defined in Eq. (2) and multiplying them by  $\mathbf{B}$ .

The quality of emulation is assessed via the mean absolute percentage error (MAPE) in the holdout set. The quality of UQ is measured by the Interval Score (IS) (Gneiting and Raftery, 2007), an intuitive scoring rule favoring small intervals, but penalizing those that fail to include the true simulator output. The IS for confidence level  $\alpha$  is  $S_\alpha^{int}(l, u; y) = (u - l) + \frac{2}{\alpha}(l - y)\mathbf{1}\{y < l\} + \frac{2}{\alpha}(y - u)\mathbf{1}\{y > u\}$ , where  $y$  is the true data value and  $l, u$  are the lower and upper bounds of the prediction interval. IS is computed for level  $\alpha = .05$  at each distance  $d$  using the 2.5 and 97.5 quantiles of the predictive samples.

The predictive metrics are shown in Figures 2b and 2c for the 100 random ensemble designs. In general, each dataset analyzed under the proposed framework will have an optimal  $m$  for predictive accuracy and UQ, which are unlikely to be the same. For these

data, we find that MAPE generally improves up to about  $m = 50$ , and can increase for larger  $m$ . The Interval score is best with a small  $m = 25$  and becomes worse when using more data for prediction. This is because increasing  $m$  reduces prediction interval widths, which are penalized by the interval score if they miss the true value. This is also seen for SVDGP where the interval score increases from  $M = 242$  to  $M = 578$ . For  $M > 98$  SVDGP has improved UQ compared to FlaGP. In other applications we have seen interval score decrease in  $m$  when prediction intervals become more narrow but still cover the data. Importantly, with the proposed framework, we have found that it is often the case that  $m = M$  is not necessary for optimal performance. For all ensemble sizes, FlaGP produces very competitive predictions to SVDGP, even for a modest neighborhood size of 25.

		$M$					
		98	242	578	1058	5618	10082
<i>Model</i>	FlaGP fit	0.089	0.167	0.276	0.258	0.152	0.272
	FlaGP pred	0.032	0.033	0.033	0.034	0.036	0.039
	SVDGP fit	13.614	39.746	186.245			
	SVDGP pred	33.274	32.722	38.231			

Table 1: Comparison of model fit and prediction time in seconds. For FlaGP, timing is given for  $m = 50$ .

FlaGP is very fast for both model fitting and prediction. For  $m = 50$ , prediction time is approximately constant over  $M$ . If we increase  $m$  to 100, prediction time only increases to about .15 seconds on average. Even for large  $M = 10082$ , model fitting, including lengthscale estimation, can be kept very fast by selecting appropriate BLHS parameters.

For the SVDGP implementation, significantly more time is needed for both fitting and prediction. It is difficult to compare the timing directly, as the SVDGP emulator is fit with MCMC, and timing is dependent on the number of samples. Here, we take a modest 1500 samples, allowing 500 for burn in, and use 100 of the final 1000 samples for prediction.

Table 1 shows that for large ensembles SVDGP would become infeasible while FlaGP can remain fast as the most significant portion of its computation time, lengthscale estimation, can be controlled. The cost of computing nearest neighbors will increase with  $M$  and  $d_x$ , which must be considered for some data. While the models presented here are

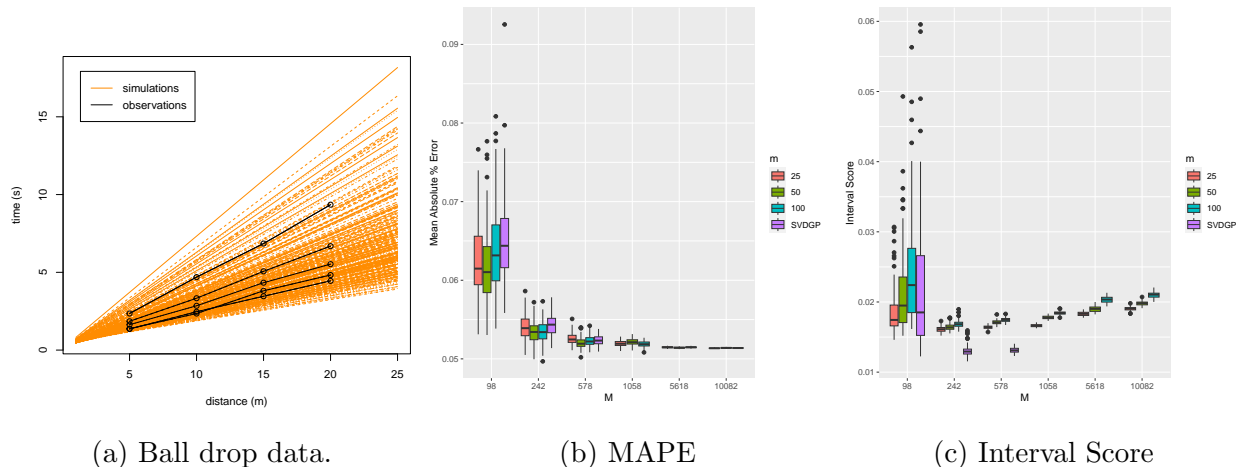


Figure 2: Panel (a) shows a representative training data ensemble in orange. Panels (b-c) show out-of-sample emulator predictive metrics over 100 ensemble designs. Predictive metrics for FlaGP are given for a number of neighborhood sizes.

relatively simple and smooth, these results indicate that the proposed method can be a competitive alternative to the full Bayesian GP approach at a fraction of the cost.

## 4 Computer Model Calibration

An important use of emulators is that of model calibration. In calibration problems there are two types of computer model inputs; controllable inputs  $\mathbf{x}$ , which are known to the experimenter, and calibration inputs  $\mathbf{t}$ , which are known for the simulation trials, but the value for the field data,  $\boldsymbol{\theta}$ , is unknown and must be estimated. The goal of computer model calibration is to use field observations and the computer model to (i) construct a predictive model for the system with uncertainty estimates; and (ii) estimate  $\boldsymbol{\theta}$ . This section describes how the fast emulator of Section 3 can be used for model calibration.

Unlike Kennedy and O’Hagan (2001) and Higdon et al. (2008), the proposed method takes a modular approach to calibration (Bayarri et al., 2009), where the emulator is fit using only the computer model data. This approach is especially relevant for the types of problems motivating this work, which tend to have small  $n$  and large  $M$ . In these cases, fitting the emulator jointly using both computer model and observed data adds theoretical complexity, but little is to be gained by the addition of a mere handful of field observations.

In some cases, the computer model is known to systematically deviate from observations. The common approach is to augment the statistical model with a so called discrepancy model to account for the systematic bias. Calibration with and without a discrepancy model requires different formulations. In Section 4.1 a calibration framework is developed for the case where the computer model is thought to be an unbiased representation of the process mean. In Section 4.2 we discuss the biased scenario.

Salter et al. (2019) show that issues can arise in calibration when the empirical basis  $\mathbf{B}$  does not represent the observations well. They propose an algorithm to rotate  $\mathbf{B}$  such that the reconstruction error for the observations is minimized. For FlaGP, this can be added as a precomputing step if needed. For the simple examples presented in this section, reconstruction error is not an issue, and for the large application dataset, we found that their methods could not be applied in a reasonable time.

## 4.1 Unbiased Calibration

Consider the setting where there are  $n$  noisy field observations, each parameterized by a vector of controllable inputs  $\mathbf{x}_i^F = (x_{i1}, \dots, x_{id_x})^T$  with corresponding functional response  $\mathbf{y}(\mathbf{x}_i^F) \in \mathbb{R}^{d_y}$ ;  $i = 1, \dots, n$ . The computer model,  $\boldsymbol{\eta}(\mathbf{x}, \mathbf{t}) \in \mathbb{R}^{d_n}$  depends not only on  $\mathbf{x}$ , but also on the calibration inputs  $\mathbf{t} = (t_1, \dots, t_{d_t})$ . With the assumption that the observed data is a noisy version of the simulator output the model for the field data is  $\mathbf{y}(\mathbf{x}_i^F) = \boldsymbol{\eta}(\mathbf{x}_i^F, \boldsymbol{\theta}) + \boldsymbol{\epsilon}$ ;  $\boldsymbol{\epsilon} \sim N(\mathbf{0}, \sigma_y^2 \mathbf{I}_n)$ . With the above formulation for  $\boldsymbol{\epsilon}$ , the vector of observations follows the conditional Gaussian distribution

$$\mathbf{y}(\mathbf{x}_i^F) \mid \boldsymbol{\eta}(\mathbf{x}_i^F, \boldsymbol{\theta}), \boldsymbol{\theta}, \sigma_y^2 \sim N(\boldsymbol{\eta}(\mathbf{x}_i^F, \boldsymbol{\theta}), \sigma_y^2 \mathbf{I}_{d_y}); \quad i = 1, \dots, n. \quad (4)$$

Each experiment is conditionally independent given the emulator and so the joint likelihood is the product of the individual likelihoods. Conditioning on the emulator allows for the i.i.d. error formulation. This results in significant computational gains for large  $d_y$  as inverting  $\sigma_y^2 \mathbf{I}$  is trivial.

For lengthscale estimation, a fast MAP approach is used because uncertainty in parameter estimates is not desired. For the calibration parameters, we sample from a Bayesian posterior distribution because uncertainty on  $\boldsymbol{\theta}$  is desired. The likelihood function is depen-

dent on parameters  $\boldsymbol{\theta}$ ,  $\sigma_y^2$ . To facilitate Bayesian inference, independent prior distributions on  $[0, 1]$  are used for each  $\theta_k$ ,  $k = 1, \dots, d_t$ . For the examples presented in this section, we use uniform priors on  $\boldsymbol{\theta}$  and an Inverse Gamma prior distribution for  $\sigma_y^2$  with parameters  $\alpha_p = 1$ , and  $\beta_p = 0.001$ . These prior distributions are chosen to closely match the default priors for SVDGP. The unnormalized posterior

$$p(\boldsymbol{\theta}, \sigma_y^2 | \cdot) \propto \prod_{i=1}^n p(\mathbf{y}(\mathbf{x}_i^F) | \boldsymbol{\eta}(\mathbf{x}_i^F, \boldsymbol{\theta}), \boldsymbol{\theta}, \sigma_y^2) \times p(\boldsymbol{\theta}) \times p(\sigma_y^2) \quad (5)$$

can be sampled using MCMC.

Algorithm 2 illustrates how to compute  $\boldsymbol{\eta}$  and evaluate the RHS of Eq. (5) for a specific  $\boldsymbol{\theta}$ ,  $\sigma_y^2$ . The algorithm is used in a joint proposal Metropolis-Hastings MCMC (MH-MCMC)

---

**Algorithm 2** Calibration without discrepancy model

---

- 1: *Predict Observations:* Use steps 1-3 in Algorithm 1 to predict observations with scaled inputs  $[\mathbf{X}_{sc}^F | \boldsymbol{\theta}_{sc}]_j$ . Using Eq. 2, draw weight vectors  $\mathbf{w}_i$  from their predictive distributions and compute emulator samples  $\boldsymbol{\eta}(\mathbf{x}_i^F, \boldsymbol{\theta}) = \mathbf{B}\mathbf{w}_i$ ,  $i = 1, \dots, n$ .
  - 2: *Log posterior density:* Evaluate Eq. (5) where the likelihood is computed from the conditional normal distribution in Eq. (4).
- 

for posterior inference on  $\boldsymbol{\theta}, \sigma_y^2$ . We found that the adaptive covariance scheme proposed by Haario et al. (2001) works very well in a variety of test problems. In our implementation the proposal covariance is adapted only during an initial burn-in phase so that samples used for convergence diagnostics and prediction use a constant proposal covariance matrix.

#### 4.1.1 Working Example: Ball Drop

Returning to the working example,  $n = 5$  noisy simulated field observations are generated from Eq. (3), and the coefficient of drag ( $C$ ) is used as a calibration input. Simulated field observations are generated using  $\mathbf{d} = (5, 10, 15, 20)$  meters,  $R_{ball} \in \{.05, .1, .15, .2, .25\}$  meters,  $C = .1$ , and  $g = 9.8$ , with random errors  $\boldsymbol{\epsilon} \sim N(0, .1^2)$ . The error variance was chosen to be approximately 5% of the variance in the simulations at  $d = 5$  meters over a range of  $M$ . Fig. 2a shows the observed data along with a representative ensemble of size  $M = 242$ .

For calibration problems it is reasonable to use 2 different neighborhood sizes, one for prediction during MCMC, and another for calibrated predictions. Let  $m_c$  be the neighborhood size used for prediction during the calibration phase, and  $m$  the neighborhood size used for calibrated predictions. For this example  $m_c = 50$  is used as we found that inference did not improve with larger  $m_c$ .

Performance metrics are evaluated using the same designs as in Section 3.2 and the observed data is held constant for all designs. The effect of the number of simulated observations is considered by running the experiment at  $M = 98$  for  $n = 5, 10$ , and 25. For both FlaGP and SVDGP, 1500 posterior samples are generated, and the first 500 are discarded as burn-in. We recognize that 1500 samples is not large in general, but it was found to be more than sufficient for the MCMC chains to appear converged and well mixed.

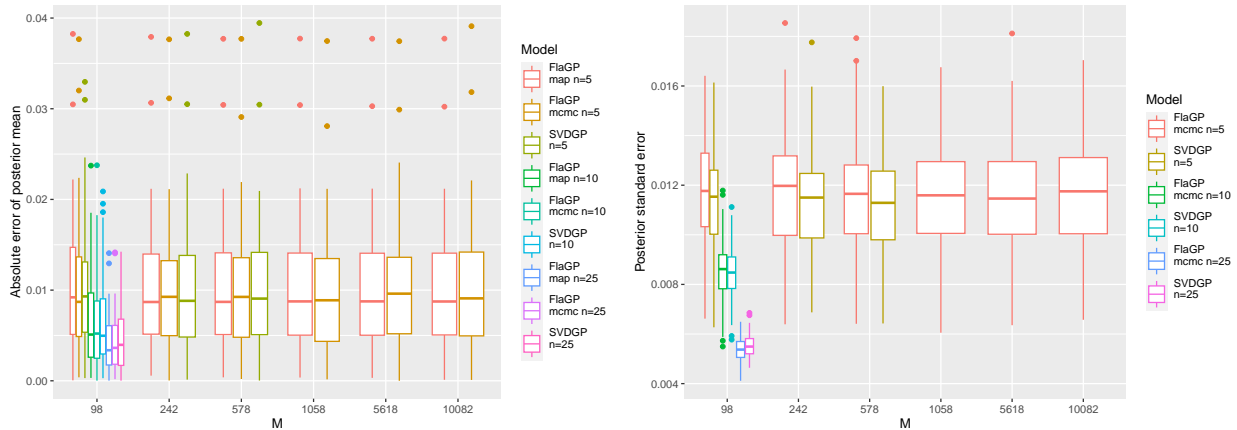
Using 100 post burn-in posterior samples the accuracy of calibration is assessed by computing the absolute difference between the posterior mean and the true  $\theta$ , the results are shown in Fig. 3a. Posterior uncertainty is shown in Fig. 3b. Both accuracy and uncertainty are fairly constant in  $m$  and  $M$ , probably due to the smoothness of the models although results over  $m$  are not shown here. Increasing  $n$  however improves accuracy and reduces uncertainty for all models. For these data, SVDGP does not improve calibration accuracy. Results are also shown for absolute error of the MAP estimate of the calibration parameters which will be discussed in detail in Section 4.3.

Fig. 3b shows that posterior uncertainty is slightly larger for FlaGP, which is expected given local prediction. Table 2 shows 95% coverage probabilities for the two MCMC methods. The FlaGP model slightly over covers, especially for small  $M$ .

		$M$					
		98	242	578	1058	5618	10082
$Model$	FlaGP	97%	97%	96%	96%	95%	96%
	SVDGP	95%	96%	93%			

Table 2: Posterior coverage probability for true calibration parameter  $\theta$  over a range of ensemble sizes. For all ensembles the same  $n = 5$  observations are used for calibration. For FlaGP,  $m = 50$  remains fixed.





(a) Absolute error of the posterior mean. (b) Posterior distribution standard deviation.

Figure 3: Accuracy of the posterior mean and posterior uncertainty for the calibration parameter in the unbiased Ball Drop example. Results are given over a range of ensemble sizes and for  $M = 98$ , the number of simulated field observations is varied.

Predictive performance is evaluated on hold out test sets. For each ensemble, 100 evaluations of Eq. (3) are generated at evenly spaced values of  $R_{ball} \in [0.025, 0.3]$  using the true value of  $C$ ,  $g = 9.8M/s^2$ , and  $\mathbf{d} = (5, 10, 15, 20)$  meters. Predictions are made using 100 post burn-in samples from the posterior  $p(\boldsymbol{\theta}, \sigma_y^2 | \cdot)$  to quantify the uncertainty in our predictions. Both the MAPE and IS are used to assess the quality of predictions from both methods which are shown in Fig. 4. Scores are also shown for the MAP approach which will be introduced in Section 4.3. The SVDGP model provides slightly improved MAPE, but FlaGP notably outperforms SVDGP in terms of IS. We found that SVDGP’s narrower calibration posteriors result in narrow prediction intervals which more often miss the true value. Increasing  $M$  does not generally improve IS.

Table 3 assesses the scalability of FlaGP. Time includes precomputing, MCMC, and prediction, averaged over the 100 runs of the study. FlaGP is significantly faster than SVDGP requiring only about 10 seconds for the largest ensemble while SVDGP takes nearly 30 minutes at  $M = 578$ .

For this simple problem the proposed model provides nearly identical predictive accuracy, and based on IS, superior uncertainty quantification.

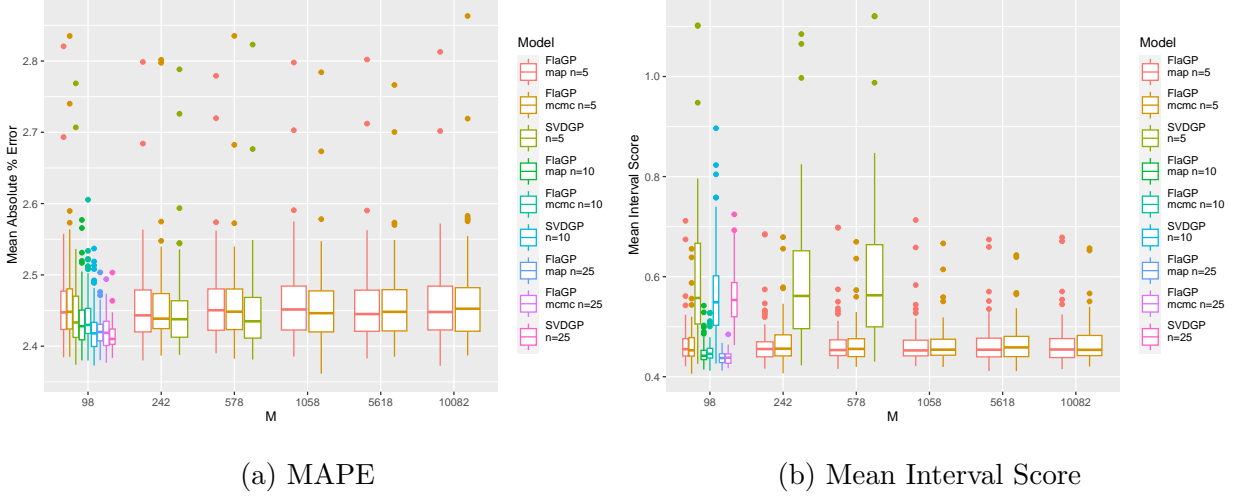


Figure 4: Predictive metrics for calibrated FlaGP emulators for the unbiased Ball Drop example. Metrics are given over a range of ensemble sizes ( $M$ ). For  $M = 98$  the number of observations ( $n$ ) is also varied.

		$M$					
		98	242	578	1058	5618	10082
$Model$	FlaGP map	0.09	0.10	0.10	0.12	0.14	0.29
	FlaGP mcmc	4.08	4.27	4.48	4.87	5.68	10.05
	SVDGP	84.08	420.09	1634.22			

Table 3: Comparison of computing time, including model fitting and prediction in seconds. For FlaGP,  $m = 50$  is kept fixed.

## 4.2 Biased Calibration

Turning to the situation where the calibrated computer model is thought to be a biased estimate of the field observations, Eq. (4) is adapted in the following way,

$$\mathbf{y}(\mathbf{x}_i^F) \mid \boldsymbol{\eta}(\mathbf{x}_i^F, \boldsymbol{\theta}), \boldsymbol{\delta}(\mathbf{x}_i^F), \boldsymbol{\theta}, \sigma_y^2 \sim N(\boldsymbol{\eta}(\mathbf{x}_i^F, \boldsymbol{\theta}) + \boldsymbol{\delta}(\mathbf{x}_i^F), \sigma_y^2 \mathbf{I}_{d_y}); i = 1, \dots, n, \quad (6)$$

where  $\boldsymbol{\delta}(\mathbf{x})$  accounts for the systematic bias between the emulator and the field observations. The emulator  $\boldsymbol{\eta}$  is modeled exactly as in equation (1), and similarly the bias is modeled as

$$\boldsymbol{\delta}(\mathbf{x}^F) = \sum_{j=1}^{p_\delta} \mathbf{k}_j v_j(\mathbf{x}^F), \quad (7)$$

where  $\{\mathbf{k}_1, \dots, \mathbf{k}_{p_\delta}\}$  is a collection of  $d_y$ -dimensional basis vectors with scalar weights  $v_j(\mathbf{x})$ . The matrix of weights is calculated as  $\mathbf{V}^T = (\mathbf{K}^T \mathbf{K})^{-1} \mathbf{K}^T \mathbf{R}_y$ , where  $\mathbf{R}_y$  is a matrix of residuals with columns  $\mathbf{y}(\mathbf{x}_i^F) - \boldsymbol{\eta}(\mathbf{x}_i^F, \boldsymbol{\theta})$ . A full GP is used to model these weights rather than laGP as  $n$  is usually small enough that computation is not an issue.

Basis vectors for the discrepancy model must be carefully selected both to achieve sensible discrepancy models, and to avoid over-fitting the relatively small number of field data points available for training the discrepancy model. One approach might be to predict the observed data using the emulator, and use the SVD of the residuals to select basis functions. We found that basis vectors selected in this way can result in severely over-fit discrepancy models, especially for small  $n$  given the flexibility of a GP. For this work, we adopt the approach of Higdon et al. (2008), by using user-selected basis functions based on prior knowledge of the discrepancy model form.

GP's for the discrepancy model are fit using the full GP implementation in the `laGP` package, which use a separable Gaussian correlation function and the same empirical Bayes procedure for estimation discussed in Section 3.1.1.

Analogous to Eq. (5), the posterior conditional density of  $\boldsymbol{\theta}, \sigma_y^2$  is

$$p(\boldsymbol{\theta}, \sigma_y^2 | \cdot) \propto \prod_{i=1}^n p(\mathbf{y}(\mathbf{x}_i) | \boldsymbol{\eta}, \boldsymbol{\delta}, \boldsymbol{\theta}, \sigma_y^2) \times p(\boldsymbol{\theta}) \times p(\sigma_y^2), \quad (8)$$

where  $p(\mathbf{y}(\mathbf{x}_i) | \boldsymbol{\eta}, \boldsymbol{\delta}, \boldsymbol{\theta}, \sigma_y^2)$  is the likelihood computed from the conditional normal distribution in Eq. (6) and  $p(\boldsymbol{\theta}), p(\sigma_y^2)$  are the prior distributions defined in Section 4.1. The following algorithm is used to compute the logarithm of the RHS of Eq. (8) for a given  $\boldsymbol{\theta}$  and  $\sigma_y^2$ . Assume a matrix  $\mathbf{K} = [\mathbf{k}_1 | \dots | \mathbf{k}_{p_\delta}]$  of basis functions for the discrepancy model has been predefined.

As in the unbiased scenario the above formula is used to compute the posterior density in a MH-MCMC. Point estimation will be discussed in the Section 4.3.

#### 4.2.1 Working Example: Ball Drop

Our working example is used to illustrate biased calibration. With a slight modification to Eq. (3), the computer model becomes a biased representation of the mean of the simulated

---

**Algorithm 3** Calibration with discrepancy model

---

- 1: *Predict Observations*: Step 1 in Algorithm 2.
  - 2: *Residuals*: Compute  $\mathbf{y}(\mathbf{x}_i^F) - \boldsymbol{\eta}(\mathbf{x}_i^F, \boldsymbol{\theta})$ ;  $i = 1, \dots, n$  and build residual matrix  $\mathbf{R}_y$ .
  - 3: *Bias precomputing*: Compute bias basis weights  $\mathbf{V}^T = (\mathbf{K}^T \mathbf{K})^{-1} \mathbf{K}^T \mathbf{R}_y$ .
  - 4: *Bias prediction*: Fit  $p_\delta$  independent separable GP models to the rows of  $\mathbf{V}^T$  and make predictions at observed inputs  $\mathbf{X}^F$ . Analogous to the emulator, sample  $\mathbf{V}$  from its predictive distributions to produce a sample of  $\boldsymbol{\delta}$ .
  - 5: *Posterior density*: Compute the log posterior density using Eq. (8) and the conditional normal likelihood in Eq. (6).
- 

field observations. In this example, computer model output is generated from

$$y(C, R_{ball}, d, g) = \frac{\text{acosh}(\exp\{Cd/R_{ball}\})}{(Cg/R_{ball})^{1/3}}, \quad (9)$$

while the observed data are still generated from Eq. (3). Changing the exponent from 1/2 to 1/3 introduces a nearly linear bias over the domain of interest. The approximately linear bias is modeled with 2 basis functions representing a linear shift. An additional layer of complexity is added here by letting  $g$  also be a calibration parameter.

For the initial exploration, computer model data was generated over a number of random designs. For each of the designs, the observed data were generated with standardized  $(C, g)$  drawn from a  $Beta(2, 2)$  distribution. Early results indicated that some of these random datasets resulted in multimodal posterior distributions for  $\boldsymbol{\theta}$ . In these situations, the emulator and discrepancy model trade-off to produce similar predictions for the observed data with very different  $\boldsymbol{\theta}, \sigma^2$ . This non-identifiability is a known phenomena when a model bias is included (Arendt et al., 2012). This is not a problem in principle, but it is a difficulty for a simulation study where we would like to ensure posterior exploration.

Ensuring thorough posterior exploration is a difficult undertaking that may require visual investigation of MCMC chains and/or running the chains significantly long such that we can be confident of convergence for these data. Visual checking is not feasible over many random designs, and in examining a few designs it was found that as many as 100000 samples might be needed to be confident in convergence without visual checks. Running a large set of models for 100000 samples would be computationally infeasible for SVDGP.

One way to encourage unimodal posteriors is to put strong priors on the process variance for the discrepancy model that encourage the model to be close to zero. The GP implementations used here integrate out the process variance, so this is not accessible. It was found that strong prior information for the discrepancy model lengthscales can alleviate multimodality in some but not all cases. For these reasons we choose to present an analysis for a single realization from our biased data generating process. A single random ensemble of size  $M = 1058$  is generated for the computer model and  $n = 10$  simulated field observations are generated with  $R_{ball} \in [.25, 1.75]$ ,  $C = .25$ , and  $g = 9.8$  with noise  $\sigma_y^2 = .1^2$ . The maximum distance is still 25 meters, but  $d_y$  is increased to 100 for both the simulations and observations.

For each model, 12,500 posterior samples are collected, and 2,500 are discarded as burn-in. Posterior density estimates from the remaining 10,000 samples are shown in Fig. 5. Note that we do not expect either model to recover the true parameter values due to the discrepancy model (Loeppky et al., 2006; Tuo and Jeff Wu, 2016). We are not surprised then, that posterior distributions for the two models have slightly different modes.

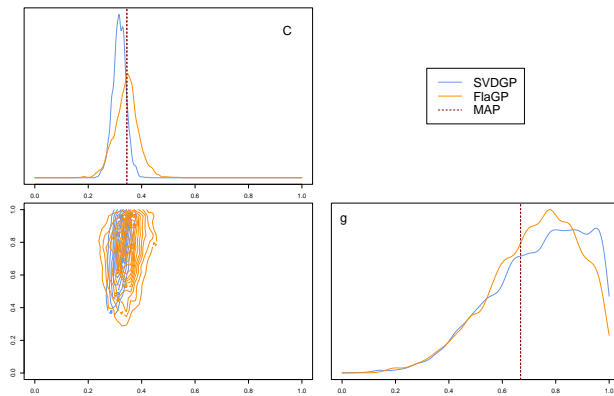


Figure 5: Posterior density estimates for the biased Ball Drop example.

Predictive performance is evaluated on a test set generated from Eq. (3). The test set is generated with 100 equally spaced values of  $R_{ball} \in [.3, 1.7]$ ,  $C = .25$ , and  $g = 9.8$ , and scores are computed with test set predictions. Score distributions are presented in Fig. 6 for the 100 prediction locations. The two models give nearly identical mean predictive accuracy and SVDGP provides only slightly improved Interval score to FlaGP at a significant increase in computation time.

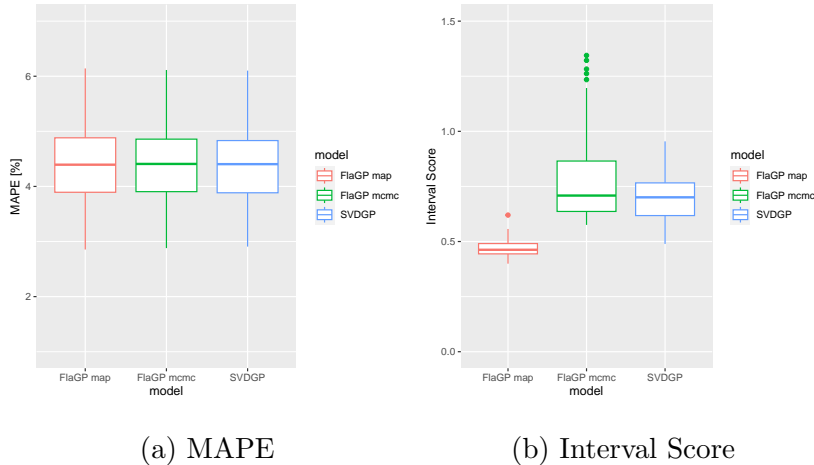


Figure 6: Comparison of predictive metrics for the biased Ball Drop example with  $M = 1058$ ,  $n = 10$ , and  $m_c = m = 50$ .

FlaGP requires just 3 seconds for precomputing, 65 seconds for the 10,000 posterior samples, and 25 seconds for prediction with  $m = 50$ . SVDGP on the other hand requires over 7 hours for fitting and 10 minutes for prediction. We argue that the small improvement in UQ may not be worth the additional computation time.

### 4.3 Fast Point Estimation

The methods presented in Sections 4.1 and 4.2 are designed for use with an MCMC sampler. Algorithms (2) and (3) cannot simply be used in an optimization routine to calculate a MAP estimate. In this section the theory required for MAP estimation with the FlaGP emulator is developed.

Equations (4) and (6) give sampling distributions for the observed data, conditional on the emulator and discrepancy, which are used to calculate the likelihood of calibration parameters. During MCMC, uncertainty in the emulator and discrepancy model is accounted for by sampling from the predictive distributions of  $\mathbf{w}(\mathbf{x}_i), \mathbf{v}(\mathbf{x}_i); i = 1, \dots, n$ . Sampling in this way makes likelihood evaluations faster because the covariance matrix is diagonal. However, sampling introduces variability to the likelihood. Repeated maximization of the posterior will lead to a distribution of MAP estimates which may be undesirable.

For a MAP estimate that is not subject to random sampling, condition observations

on the mean and variance of the emulator and discrepancy models. Equations (10) and (11) present new conditional sampling distributions for each of the  $n$  observations. For the unbiased and biased computer model they are respectively

$$\mathbf{y}(\mathbf{x}_i^F) \mid \mathbf{m}_{wi}, \boldsymbol{\Sigma}_{wi}, \boldsymbol{\theta}, \sigma_y^2 \sim N(\mathbf{B}\mathbf{m}_{wi}, \sigma_y^2 \mathbf{I}_{d_y} + \mathbf{B}\boldsymbol{\Sigma}_{wi}\mathbf{B}^T) \quad (10)$$

$$\mathbf{y}(\mathbf{x}_i^F) \mid \mathbf{m}_{wi}, \boldsymbol{\Sigma}_{wi}, \mathbf{m}_{vi}, \boldsymbol{\Sigma}_{vi}, \boldsymbol{\theta}, \sigma_y^2 \sim N(\mathbf{B}\mathbf{m}_{wi} + \mathbf{K}\mathbf{m}_{vi}, \sigma_y^2 \mathbf{I}_{d_y} + \mathbf{B}\boldsymbol{\Sigma}_{wi}\mathbf{B}^T + \mathbf{K}\boldsymbol{\Sigma}_{vi}\mathbf{K}^T), \quad (11)$$

where  $\mathbf{m}_{wi}$  and  $\boldsymbol{\Sigma}_{wi}$  are the mean and variance for the emulator predictions at  $\mathbf{x}_i^F$ . Similarly  $\mathbf{m}_{vi}$  and  $\boldsymbol{\Sigma}_{vi}$  are the mean and variance for the discrepancy model prediction at  $\mathbf{x}_i^F$ . Conditioning in this way eliminates the variability in the likelihood at the cost of a non-diagonal  $d_y \times d_y$  covariance matrix, which can be very large. Fortunately, if we approximate the Student-t predictive distributions in equation 2 with a Normal distribution, and use *Result 1.* from Higdon et al. (2008), the matrix inversion cost is reduced from  $\mathcal{O}(d_y^3)$  to  $\mathcal{O}((n(p_\eta + p_\delta))^3)$ . The details of this can be found in Appendix A. The Normal approximation to the Student-t will be very good for the large ensembles we consider. However, the approximation may cause underestimation of the predictive variance for the discrepancy model, especially for small  $n$ . This is compensated for by slightly larger estimates of  $\sigma_y^2$ . By using these sampling distributions to redefine the conditional likelihoods  $p(\mathbf{y}(\mathbf{x}_i)|\cdot)$ , posterior estimation can be efficiently carried out. In the unbiased scenario, this is achieved by letting Eq. (5) be the objective function in the optimization algorithm. For this work, the algorithm NOMAD (Audet et al., 2008) is used for optimization. Similarly, in the biased scenario, Eq. (8) is employed for the same purpose.

### 4.3.1 Working Example: Ball Drop

In the unbiased ball drop example, Fig. 3a shows that the MAP approach is as good as both the proposed MCMC approach and SVDGP in its ability to infer the true calibration parameter. Fig. 4a shows that the predictive mean from the MAP approach is on par with the other two methods. Fig. 4b shows that UQ with the MAP approach is also similar to the MCMC approach, and is better than SVDGP for these data. Table 3 shows that the MAP approach is extremely fast and scales well with  $M$ .

For the biased ball drop example, Fig. 6 shows that the MAP approach is again very

competitive. While these results are encouraging for fast emulation and calibration without MCMC, there remains the drawback of no uncertainty in the estimates of the calibration parameters, which calls the overall UQ into question. Furthermore, this approach cannot give insight or quantify uncertainty associated with multimodal posterior distributions.

## 5 Al-5083 Analysis

The FlaGP methodology is applied to the application dataset described in Section 2. Recall that an ensemble of  $M = 20000$  runs from the FLAG simulator is available for 3 shots representing different flyer plate and sample thickness. The output of each of these runs is a velocity curve over time. A single experimental velocity curve is also available for each shot. As in Walters et al. (2018), the 3 shots are emulated jointly resulting in a functional response of length  $d_y = 1500$ . The shots could also be modeled with 3 separate emulators, with a product likelihood over the emulators used for calibration, however we choose to follow the joint emulation approach of Walters et al. (2018). This ensemble is sufficiently large so that the SVDGP method is computationally infeasible to apply, however a tractable analysis can be done with the proposed method. In Section 5.0.1 we show that the proposed emulator can quickly and accurately emulate FLAG, and in Section 5.0.2 we present a fast calibration that accurately predicts the observed data. This application is representative of the type used in production at materials science facilities. For these applications the FlaGP methodology provides calibration that can be updated very quickly in the presence of additional experimental data.

### 5.0.1 Emulation

To assess emulator accuracy, an FlaGP model is fit to 19000 simulations, and 1000 are kept as prediction holdout. To avoid extrapolation, which we normally do not recommend, the test set is randomly selected from within the 2.5% and 97.5% quantiles of the input distributions.

The first step in fitting the emulator is computing basis functions. Given the large



ensemble data matrix, a random svd (RSVD) (Halko et al., 2011) is used rather than a full SVD. The RSVD approximates the first 7 basis vectors in less than 3 seconds, 20 times faster than a full SVD. This number of basis vectors was chosen so that over 99% of the variability in the data is captured. For these data the RSVD basis vectors are an extremely accurate representation of the full SVD basis.

Next, the input space must be scaled for fast prediction. Stratified random sampling is used to select subsets of the ensemble for lengthscale estimation. Parameters  $m_{est}$  and  $r_{est}$  must be chosen, and a reasonable approach is to select small initial values, resulting in fast estimation. Parameter values can then be increased if predictive metrics indicate that improvement is needed. For these data initial values of  $m_{est} = 256$  and  $r_{est} = 25$  are used. Including the RSVD, the total fitting time for this model is just 2 minutes.

To illustrate emulator accuracy on holdout data, we start with a relatively small prediction neighborhood size of  $m = 50$ , which affords prediction at the 1000 hold out locations in just 3 seconds. Table 4 shows shot specific Root Mean Squared Error (RMSE) averaged over the velocity curve. RMSE is used as the predictive scoring metric rather than relative error because there are many velocity values at or near zero, which presents issues for relative error calculations. Normalized RMSE was also considered, but lacks the same level of interpretability. The first 3 columns of row 1 in the table show RMSE for the described emulator with  $m_{est} = 256$ ,  $r_{est} = 25$ , and  $m = 50$ . The other entries in the table will be discussed later. Velocity curves range from 0 – 500m/s, so RMSE in the range of 3-6 m/s is quite small. The fact that RMSE for shot 106 is much larger than for shot 104 does not indicate that it is poorly emulated by comparison, in fact, normalized RMSE’s indicate that shot 106 is the most accurately predicted. Dividing the RMSE values of 3.23, 4.88, and 5.26 by mean shot velocity gives relative RMSE’s of 0.023, 0.025, and 0.018.

The emulator described above requires a very small computational budget. A larger budget is also considered by increasing  $m_{est}$  and  $m$ . Table 4 shows emulator prediction accuracy for  $m_{est} \in \{512, 1024\}$  and  $m \in \{100, 250\}$ . The results show that there is some gain in performance by increasing these parameters, however, these gains may not be of practical significance given the computational cost. For  $m_{est} = 512$ , 17 minutes

		$m_{est}, shot\#$								
		256			512			1024		
		$104$	$105$	$106$	$104$	$105$	$106$	$104$	$105$	$106$
$m$	50	3.23	4.88	5.26	3.11	4.60	5.11	3.10	4.70	5.02
	100	3.16	4.80	5.19	3.14	4.50	5.08	3.21	4.70	5.07
	250	3.04	4.44	4.91	3.00	4.26	4.95	3.01	4.35	4.93

Table 4: Average RMSE ( $m/s$ ) over 1000 hold-out velocity profiles for each of the 3 shots. All combinations of  $m_{est} \in \{256, 512, 1024\}$ ,  $m \in \{50, 100, 250\}$  are shown.

are needed for precomputing, and for  $m_{est} = 1024$ , 4 hours. For prediction,  $m = 250$  increases prediction time to 40 seconds. The results in Table 4 indicate that the FLAG simulator can be accurately emulated with a very small computational budget and only small improvements are had with an increased budget.

### 5.0.2 Calibration

In this section we use the emulation methods described above, along with the experimental velocity curves to calibrate the 11 input parameters. Section 5.0.1 informs reasonable choices of tuning parameters  $m_{est}$ ,  $r_{est}$ , and  $m$ . Again, 7 basis vectors are used, computed with the RSVD, and stratified random sampling is used to select subsets for lengthscale estimation. An analysis with a moderate computation budget was done using  $m_{est} = 512$ ,  $r_{est} = 25$ , and  $m_c = 50$ . A total of 100000 MCMC samples are collected and the first 25000 are used for proposal covariance adaptation and discarded. The total cost of precomputing and MCMC calibration is 2 hours. Density estimates from the 75000 post burn-in samples are shown in Fig. 7, and a notable reduction in prior uncertainty is seen for most of the parameters.

This analysis uses conservative choices of  $m_{est}$ ,  $r_{est}$ , and the number of MCMC samples to ensure model convergence and accurate lengthscale estimation. A significantly more efficient analysis is done with  $m_{est} = 256$ ,  $r_{est} = 10$ , and  $m_c = 50$ , reducing precomputing time to less than 1 minute. By collecting only 10000 MCMC samples (using the first 5000 for covariance adaption), the total time is reduced to just 11.5 minutes. A fast MAP

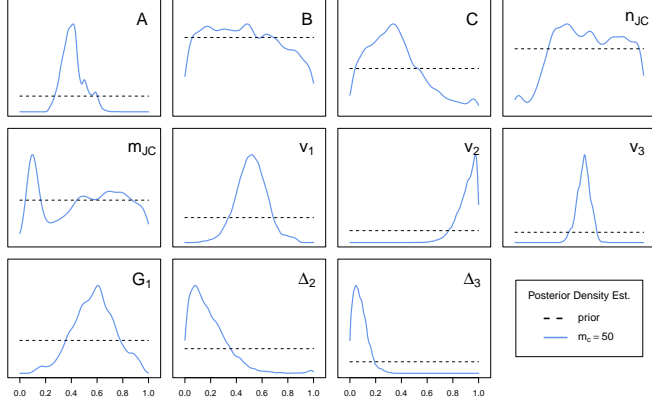


Figure 7: Posterior density estimates of the calibration parameters for  $m_c = 50$ .

estimate of the calibration parameters is also considered, which takes only 90 seconds with 7 random restarts of the optimizer, selected to match available compute cores.

The first row of Fig. 8 shows posterior predictive means and 95% intervals for the 3 observed velocity profiles using the moderate budget analysis with  $m = 50$  for prediction. All 3 shots are well predicted, and are mostly contained within the prediction intervals. The second and third rows show predictions for the faster MCMC and MAP models. Visually, there is very little difference between these predictions. The RMSE, IS, and computing time for all three models are given in Table 5. The slower model does not score significantly better than the more efficient models, which was also seen in Section 5.0.1. The extremely fast MAP approach is competitive with MCMC in both predictive accuracy and uncertainty quantification.

		RMSE			Interval Score			Total Compute
		104	105	106	104	105	106	
<i>Model</i>	MCMC: Moderate budget	3.68	4.24	5.23	19.91	20.72	32.03	2.10 hours
	MCMC: Small budget	3.21	4.20	5.55	18.67	19.57	33.83	11.45 minutes
	MAP	3.85	4.50	6.21	19.77	21.53	32.75	2.38 minutes

Table 5: Calibrated prediction RMSE, IS, and computing time for 3 models of varied computational budget.

For this analysis we can afford a moderate computational budget as model fitting and

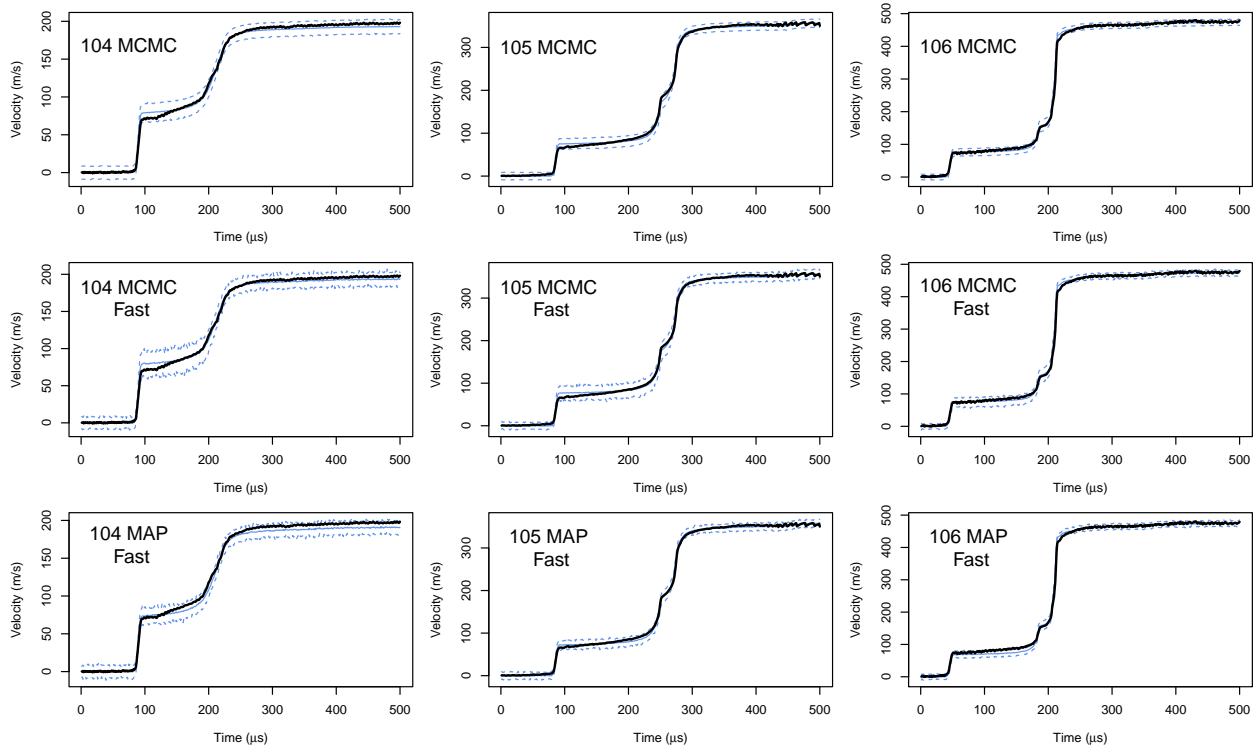


Figure 8: Posterior mean and 95% prediction intervals for the observed shots using 3 modeling procedures. The top row shows predictions from an MCMC calibration with a moderate budget (2 hours), predictions from a faster MCMC calibration (12 minutes) are shown in row 2, and MAP calibration predictions in the bottom row (3 minutes).

parameter calibration is only done once. However, an important takeaway is the relative success of the small budget MCMC and MAP calibration. For applications where new data arrives sequentially, the emulator and calibration can be updated rapidly without a notable loss in prediction accuracy or UQ.

## 6 Discussion

This work introduces FlaGP, an efficient implementation of **laGP** for the emulation and calibration of computer models with functional response. FlaGP incorporates local GP's, modularization, and input scaling to enhance scalability compared to the established GP methodology described in Higdon et al. (2008). Unlike a fully Bayesian model that utilizes

all data at each step, FlaGP offers improved efficiency while maintaining accuracy. For small datasets, the SVDGP may be preferable, however, we are frequently presented with problems for which SVDGP is computationally infeasible. Through a working example it is demonstrated that FlaGP can produce competitive predictions, and may even be preferable in terms of uncertainty quantification for some data.

Importantly, it is shown that SVDGP becomes quickly infeasible in computation time with increasing  $M$ . The FlaGP model can be fit with nearly any computational budget by selecting an appropriate prediction neighborhood size and subset size for lengthscale estimation. This is illustrated in Section 5.0.1 where model fitting and accurate prediction at 1000 points can be achieved for a large ensemble ( $M = 19000$ ) in just 2 minutes.

In Section 5.0.2 the FlaGP methodology is exercised on a large calibration problem where the SVDGP would be infeasible. The proposed methodology is able to constrain the input parameters using a single observation and accurately predict experiment using calibrated parameters. It is shown that a small computational budget of just 11.5 minutes is sufficient to provide accurate calibrated predictions that are very competitive with an FlaGP model using a larger budget of 2 hours. Furthermore, the very fast MAP approach developed for FlaGP provides competitive calibrated predictions in just 2.4 minutes. While this method does not provide uncertainty in the calibration parameter estimates, it may be a useful tool in situations where a fast point estimate is sufficient.

FlaGP is developed with truly large ensemble datasets in mind. For sufficiently large  $M * d_y$  computing the SVD becomes prohibitive. In this work only data with  $d_y \leq 1500$  are explored however there exist many applications such as spatial or time series data where  $d_y$  is much larger. In Section 5 we show that the RSVD can significantly reduce the time required for this precomputing step, and for those data, the RSVD is extremely accurate.

In the examples presented here, we have chosen not to incorporate strong prior information about the parameters, but it is worth noting that incorporating stronger information may be beneficial. For example, outputs are scaled to have unit variance, so it is expected that  $\sigma_y^2 \ll 1$ . If the emulator is expected to capture a significant proportion of this variability, say 90%, then it may be beneficial to design a prior for  $\sigma_y^2$  with nearly all of its

mass below one, and a peak near 0.1.

## Appendix A Efficient likelihood calculation

Notice that Eq. (10) can be rearranged as  $\mathbf{y}^F(\mathbf{x}_i^F) - \mathbf{B}\mathbf{m}_{wi} \sim N(\mathbf{0}_{d_y}, \mathbf{B}\Sigma_{i\eta}\mathbf{B}^T) + N(\mathbf{0}_{d_y}, \sigma_y^2\mathbf{I}_{d_y})$  and similarly Eq. (11) as  $\mathbf{y}^F(\mathbf{x}_i^F) - [\mathbf{B}; \mathbf{K}] \begin{bmatrix} \mathbf{m}_{wi} \\ \mathbf{m}_{vi} \end{bmatrix} \sim N(\mathbf{0}_{d_y}, \begin{bmatrix} \mathbf{B}\Sigma_{wi}\mathbf{B}^T & \mathbf{0} \\ \mathbf{0} & \mathbf{K}\Sigma_{vi}\mathbf{K}^T \end{bmatrix}) + N(\mathbf{0}_{d_y}, \sigma_y^2\mathbf{I}_{d_y})$ . Defining  $\lambda_y = \frac{1}{\sigma_y^2}$  and  $\mathbf{r}(\mathbf{x}_i) = \mathbf{y}^F(\mathbf{x}_i^F) - \mathbf{B}\mathbf{m}_{wi}$ , *Result 1.* implies that the unnormalized log likelihood in the unbiased calibration case can be written as

$$\begin{aligned} ll(\mathbf{r}(\mathbf{x}_i)) &\propto -\frac{1}{2} \left( \log(|\sigma_y^2\mathbf{I}|) + \log(|\lambda_y\mathbf{B}^T\mathbf{B}|) + \mathbf{r}(\mathbf{x}_i)^T \left[ \lambda_y\mathbf{I} - \lambda_y\mathbf{B}(\lambda_y\mathbf{B}^T\mathbf{B})^{-1}\mathbf{B}^T\lambda_y \right] \mathbf{k}_i \right) + ll(\boldsymbol{\gamma}_i) \\ &= -\frac{1}{2} \left( (d_y - \text{Rank}(\mathbf{B}))\log(\sigma_y^2) + \log(|\mathbf{B}^T\mathbf{B}|) + \lambda_y\mathbf{r}(\mathbf{x}_i)^T (\mathbf{I} - \mathbf{B}(\mathbf{B}^T\mathbf{B})^{-1}\mathbf{B}^T)\mathbf{r}(\mathbf{x}_i) \right) + ll(\boldsymbol{\gamma}_i), \end{aligned} \quad (12)$$

where  $\boldsymbol{\gamma}_i = (\mathbf{B}^T\mathbf{B})^{-1}\mathbf{B}^T\mathbf{r}(\mathbf{x}_i) \implies \boldsymbol{\gamma}_i \sim N(\mathbf{0}, \Sigma_{wi} + \sigma_y^2(\mathbf{B}^T\mathbf{B})^{-1})$ . For the biased scenario, define  $\mathbf{C} = [\mathbf{B}; \mathbf{K}]$  and  $\mathbf{r}(\mathbf{x}_i) = \mathbf{y}_i^F(\mathbf{x}_i^F) - \mathbf{C} \begin{bmatrix} \mathbf{m}_{wi} \\ \mathbf{m}_{vi} \end{bmatrix}$ . The biased log-likelihood can be computed using Eq. (12) replacing  $\mathbf{B}$  with  $\mathbf{C}$ , and updating  $\mathbf{r}(\mathbf{x}_i)$  and  $\boldsymbol{\gamma}_i \sim N(\mathbf{0}, \begin{bmatrix} \Sigma_{wi} & \mathbf{0} \\ \mathbf{0} & \Sigma_{vi} \end{bmatrix} + \sigma_y^2(\mathbf{C}^T\mathbf{C})^{-1})$  to reflect the addition of the discrepancy model. The log posterior is then  $\log(p(\boldsymbol{\theta}|\cdot)) \propto \sum_{i=1}^n ll(\mathbf{r}(\mathbf{x}_i)) + \log(p(\boldsymbol{\theta}))$ .

## References

- Arendt, P. D., Apley, D. W., and Chen, W. (2012). Quantification of model uncertainty: Calibration, model discrepancy, and identifiability. *Journal of Mechanical Design*, 134:100908.
- Audet, C., Béchar, V., and Digabel, S. L. (2008). Nonsmooth optimization through mesh adaptive direct search and variable neighborhood search. *Journal of Global Optimization*, 41(2):299–318.
- Bayarri, M. J., Berger, J. O., and Liu, F. (2009). Modularization in bayesian analysis, with emphasis on analysis of computer models. *Bayesian Analysis*, 4(1):119 – 150.

- Boteler, J. M. and Dandekar, D. P. (2006). Dynamic response of two strain-hardened aluminum alloys. *Journal of Applied Physics*, 100(5):054902.
- Burton, D. E. (2007). Lagrangian hydrodynamics in the flag code. Technical report, Lawrence Livermore National Lab.(LLNL), Livermore, CA (United States).
- Chang, W., Haran, M., Olson, R., and Keller, K. (2014). Fast dimension-reduced climate model calibration and the effect of data aggregation. *The Annals of Applied Statistics*, 8(2):649 – 673.
- Constantine, P. G., Dow, E., and Wang, Q. (2014). Active subspace methods in theory and practice: Applications to kriging surfaces. *SIAM Journal on Scientific Computing*, 36(4):A1500–A1524.
- Datta, A., Banerjee, S., Finley, A. O., and Gelfand, A. E. (2016). Hierarchical nearest-neighbor gaussian process models for large geostatistical datasets. *Journal of the American Statistical Association*, 111(514):800–812. PMID: 29720777.
- Francom, D. C., Sansó, B., Bulaevskaya, V., Lucas, D. D., and Simpson, M. (2019). Inferring atmospheric release characteristics in a large computer experiment using bayesian adaptive splines. *Journal of the American Statistical Association*, 114:1450 – 1465.
- Gattiker, J., Klein, N., Hutchings, G., and Lawrence, E. (2020). lanl/sepia: v1.1.
- Gneiting, T. and Raftery, A. E. (2007). Strictly proper scoring rules, prediction, and estimation. *Journal of the American Statistical Association*, 102(477):359–378.
- Gramacy, R. B. (2016). lagp: Large-scale spatial modeling via local approximate gaussian processes in r. *Journal of Statistical Software*, 72(1):1–46.
- Gramacy, R. B. and Apley, D. W. (2015). Local gaussian process approximation for large computer experiments. *Journal of Computational and Graphical Statistics*, 24(2):561–578.

- Gramacy, R. B., Bingham, D., Holloway, J. P., Grosskopf, M. J., Kuranz, C. C., Rutter, E., Trantham, M., and Drake, R. P. (2015). Calibrating a large computer experiment simulating radiative shock hydrodynamics. *The Annals of Applied Statistics*, 9(3):1141 – 1168.
- Haario, H., Saksman, E., and Tamminen, J. (2001). An adaptive metropolis algorithm. *Bernoulli*, 7(2):223 – 242.
- Halko, N., Martinsson, P. G., and Tropp, J. A. (2011). Finding structure with randomness: Probabilistic algorithms for constructing approximate matrix decompositions. *SIAM Review*, 53(2):217–288.
- Higdon, D., Gattiker, J., Williams, B., and Rightley, M. (2008). Computer model calibration using high-dimensional output. *Journal of the American Statistical Association*, 103(482):570–583.
- Hsu, G. (2019). *Fast emulation and calibration of large computer experiments with multivariate output*. PhD thesis, Simon Fraser University.
- Johnson, G. R. and Cook, W. H. (1983). Seventh international symposium on ballistics, the hague, the netherlands. pages 541 – 547.
- Katzfuss, M., Guinness, J., and Lawrence, E. (2022). Scaled vecchia approximation for fast computer-model emulation. *SIAM/ASA Journal on Uncertainty Quantification*, 10(2):537–554.
- Kaufman, C. G., Bingham, D., Habib, S., Heitmann, K., and Frieman, J. A. (2011). Efficient emulators of computer experiments using compactly supported correlation functions, with an application to cosmology. *The Annals of Applied Statistics*, 5(4):2470 – 2492.
- Kennedy, M. and O’Hagan, A. (2001). Bayesian calibration of computer models (with discussion). *J. R. Statist. Soc. B*, 63:425–464.



- Liu, Y. (2014). *Recent advances in computer experiment modeling*. PhD thesis, Rutgers University.
- Loeppky, J., Bingham, D., and Welch, W. (2006). Computer model calibration or tuning in practice. *University of British Columbia, Vancouver, BC, Canada*.
- Ma, P., Mondal, A., Konomi, B. A., Hobbs, J., Song, J. J., and Kang, E. L. (2022). Computer model emulation with high-dimensional functional output in large-scale observing system uncertainty experiments. *Technometrics*, 64(1):65–79.
- Rumsey, K. N., Huerta, G., and Derek Tucker, J. (2023). A localized ensemble of approximate gaussian processes for fast sequential emulation. *Stat*, 12(1):e576.
- Sacks, J., Welch, W. J., Mitchell, T. J., and Wynn, H. P. (1989). Design and analysis of computer experiments. *Statistical Science*, 4(4):409 – 423.
- Salter, J. M., Williamson, D. B., Scinocca, J., and Kharin, V. (2019). Uncertainty quantification for computer models with spatial output using calibration-optimal bases. *Journal of the American Statistical Association*, 114(528):1800–1814.
- Stein, M. L., Chi, Z., and Welty, L. J. (2004). Approximating likelihoods for large spatial data sets. *Journal of the Royal Statistical Society: Series B (Statistical Methodology)*, 66(2):275–296.
- Sun, F., Gramacy, R. B., Haaland, B., Lawrence, E., and Walker, A. (2019). Emulating satellite drag from large simulation experiments. *SIAM/ASA Journal on Uncertainty Quantification*, 7(2):720–759.
- Tang, B. (1993). Orthogonal array-based latin hypercubes. *Journal of the American Statistical Association*, 88(424):1392–1397.
- Tuo, R. and Jeff Wu, C. F. (2016). A theoretical framework for calibration in computer models: Parametrization, estimation and convergence properties. *SIAM/ASA Journal on Uncertainty Quantification*, 4(1):767–795.

- Vecchia, A. V. (1988). Estimation and model identification for continuous spatial processes. *Journal of the Royal Statistical Society. Series B (Methodological)*, 50(2):297–312.
- Walters, D. J., Biswas, A., Lawrence, E. C., Francom, D. C., Luscher, D. J., Fredenburg, D. A., Moran, K. R., Sweeney, C. M., Sandberg, R. L., Ahrens, J. P., and Bolme, C. A. (2018). Bayesian calibration of strength parameters using hydrocode simulations of symmetric impact shock experiments of al-5083. *Journal of Applied Physics*, 124(20).
- Zhang, R. C., Lin, D., and Ranjan, P. (2018). Local gaussian process model for large-scale dynamic computer experiments. *Journal of Computational and Graphical Statistics*, 27(4):798–807.

# Supplement: Fast Emulation and Modular Calibration for Simulators with Functional Response

May 28, 2024

## 1 FlaGP Algorithm in detail

A detailed algorithm for the methods presented in this paper is given here, and are implemented in the R package `FlaGP`. Algorithm 1. in the manuscript provides an outline for fitting the emulator and making predictions. Algorithms 2. & 3. define the procedures for using predictions from the emulator in a modular calibration framework. The purpose of these Supplemental algorithms is to provide more detail that should be sufficient to implement the methods from scratch.

---

**Algorithm 1** Fast Emulator fit and Prediction

---

**Phase 1: Fit Emulator**

---

### Precomputing 1: Data Setup

- 1: Scale input matrix  $\mathbf{X} \in \mathbb{R}^{M \times d_x}$  to unit Hypercube  $[0, 1]^{d_x}$ .
- 2: Center output Matrix  $\mathbf{Z} \in \mathbb{R}^{d_y \times M}$  by subtracting the mean at each functional index. Optionally, scale  $\mathbf{Z}$  to have unit variance.
- 3: Compute Singular Value Decomposition  $\mathbf{Z} = \mathbf{U}\mathbf{D}\mathbf{V}^T$
- 4: Select  $p_\eta$ , the number of basis components to keep for modeling, by choosing a minimum desired proportion of variability in  $\mathbf{Z}$  to be explained by the decomposition (commonly .95). The proportion of variance explained by each singular vector is  $\mathbf{d}^2 / \sum \mathbf{d}^2$  where  $\mathbf{d}$  is the  $d_y$  vector of singular values along the diagonal of  $\mathbf{D}$ .

- 5: Define the low rank basis  $\mathbf{Z} \approx \mathbf{B}\mathbf{W}(\mathbf{X})$  where  $\mathbf{B}$  is the first  $p_\eta$  columns of  $\mathbf{U}\mathbf{D}/\sqrt{M}$  and  $\mathbf{W}(\mathbf{X})$  is the first  $p_\eta$  rows of  $\mathbf{V}^T\sqrt{M}$ .

**Precomputing 2: Estimate GP correlation parameters**

- 6: *Option 1:* For each of the  $p_\eta$  rows in  $\mathbf{W}(\mathbf{X})$ , estimate correlation lengths using the `laGP` function `blhs.loop` with  $d_{est}$  divisions on each coordinate in  $\mathbf{X}$  and  $r_{est}$  bootstrap samples. This function uses Bootstrapped Block Latin hypercube sampling to define  $r_{est}$  data subsets, then estimates correlation lengths for each subset using an Empirical Bayes MAP estimation procedure. The median over bootstrap subsets are given as the estimates  $\{\hat{\mathbf{l}}\}_{p_\eta}$ .
- 7: *Option 2:* Sample  $r_{est}$  bootstrap subsets of size  $m_{est}$  using stratified or simple random sampling. Use the `laGP` functions `newGPsep` and `mleGPsep` to estimate correlation lengths using the same Empirical Bayes procedure for each bootstrap subset. Take the median over subsets to estimates  $\{\hat{\mathbf{l}}\}_{p_\eta}$ .

The computation time of these estimation procedures is dependent on  $d_{est}$  or  $m_{est}$  and  $r_{est}$ . In practice, we recommend setting  $d_{est}$  small and  $m_{est}, r_{est}$  large if computational budget allows.

**Precomputing 3: Stretch and Compress inputs**

- 8: Given estimates  $\hat{\mathbf{l}}_j; j = 1, \dots, p_\eta$ , defined stretched and compressed inputs

$$\mathbf{X}_j^{sc} = \mathbf{X} / \sqrt{\hat{\mathbf{l}}_j}$$

where division is column-wise, that is, the  $i$ 'th column of  $\mathbf{X}_j^{sc}$ , denoted  $\mathbf{x}_{ij}^{sc}$  is computed by dividing the  $i$ 'th column of  $\mathbf{X}$ ,  $\mathbf{x}_{ij}$ , by the  $i$ 'th lengthscale estimate for the  $j$ 'th basis component  $\hat{l}_{ij}$ .

$$\mathbf{x}_{ij}^{sc} = \mathbf{x}_{ij} / \hat{l}_{ij}$$

---

**Phase 2: Predictions from fitted Emulator**

---

**Scale Prediction input  $\mathbf{x}$**

9: Compute  $p_\eta$  scaled prediction inputs

$$\mathbf{x}_j^{sc} = \mathbf{x} / \sqrt{\hat{\mathbf{l}}_j}$$

- .
- 10: Build nearest neighbor training datasets: Define training data for the  $j$ 'th basis component model, as the  $m$  nearest neighbor inputs to  $\mathbf{x}_j^{sc}$  in  $\mathbf{X}_j^{sc}$  along with their associated basis weights from  $\mathbf{W}(\mathbf{X})$ . Nearest neighbors are computed using a fast K-d tree algorithm implemented in the R function `FNN::get.knnx()`.
  - 11: Sample from predictive distribution: Training data defines predictive distributions (Equation 2.) for for  $w(\mathbf{x}_j^{sc})$
  - 12: Combine predictions from  $p_\eta$  basis models: To compute predictions in function space, propagate predictions through the basis vectors,

$$\mathbf{z}(\mathbf{x}) = \sum_{i=1}^{p_\eta} \mathbf{b}_i w(\mathbf{x}_i^{sc})$$

---

---

**Algorithm 2** Modular Calibration with FlaGP Emulator
 

---

**Require:** *Fitted Emulator* Use Phase 1 of Algorithm 1 to fit the modular emulator. In this case, the two types of inputs  $\mathbf{X}$ ,  $\mathbf{T}$ , require  $d_x + d_t$  lengthscale parameters to be estimated for each of the  $p_\eta$  models. Denote two sets of lengthscale parameters as  $\{\hat{\mathbf{l}}_x\}_{p_\eta}$ ,  $\{\hat{\mathbf{l}}_t\}_{p_\eta}$ .

**Predict Field Observations at  $\theta = t$**

- 1: Emulator Prediction: For stretched and compressed inputs  $\{\mathbf{X}_F^{sc}\}_{p_\eta}$  and  $\{\mathbf{t}^{sc}\}_{p_\eta}$  take a sample from the predictive distribution of  $\mathbf{w}_i(\{\mathbf{X}_F^{sc}\}_{p_\eta}, \{\mathbf{t}^{sc}\}_{p_\eta})$   $i = 1, \dots, n$  using the procedure in Phase 2 of Algorithm 1. Denote the sample from the predictive distribution of the  $i$ 'th observation as  $\tilde{\mathbf{w}}_i$ . Compute matrix of residuals  $\mathbf{R} = \mathbf{Y} - \tilde{\mathbf{W}}\mathbf{B}$ .
- 2: Discrepancy Model: With user-defined discrepancy basis matrix  $\mathbf{D}$ , compute projected residual matrix  $\mathbf{V} = (\mathbf{D}^T\mathbf{D})^{-1}\mathbf{D}^T\mathbf{R}$ . Fit independent full Gaussian Process models to the rows of  $\mathbf{V}$ , each with input matrix  $\mathbf{X}_F$  using `laGP` functions `newGPsep` and `mleGPsep`. Stretched and compressed inputs are not used for the discrepancy model because lengthscale estimates are computed w.r.t outputs  $\mathbf{W}$ , not  $\mathbf{V}$ , so lengthscale parameters must be estimated. Draw a sample from the predictive distribution of the discrepancy model at each of  $n$  the observed inputs  $\mathbf{X}_F$ . Denote the samples as  $\tilde{\mathbf{v}}_i$ .

**Compute posterior probability of  $\theta = t$**

- 3: Compute log-posterior: According to the model

$$\mathbf{y}_i(\mathbf{x}_i^F) \sim N(\boldsymbol{\eta}(\mathbf{x}_i^F, \boldsymbol{\theta}) + \boldsymbol{\delta}(\mathbf{x}_i^F), \sigma_y^2 \mathbf{I})$$

compute posterior

$$p(\mathbf{t}, \sigma_y^2 | \cdot) \propto -0.5 \left( nd_y \log(\sigma_y^2) + \frac{1}{\sigma_y^2} \sum_i (\mathbf{r}_1^2, \dots, \mathbf{r}_n^2)(\mathbf{r}_1^2, \dots, \mathbf{r}_n^2)^T \right) \times \pi(\mathbf{t}) \times \pi(\sigma_y^2)$$

where  $\mathbf{r}_i = \mathbf{y}_i(\mathbf{x}_i^F) - \boldsymbol{\eta}(\mathbf{x}_i^F, \boldsymbol{\theta}) - \boldsymbol{\delta}(\mathbf{x}_i^F) = \mathbf{y}_i(\mathbf{x}_i^F) - \tilde{\mathbf{w}}_i\mathbf{B} - \tilde{\mathbf{v}}_i\mathbf{D}$ .

- 4: Repeat steps 1-3 in an MCMC loop to sample from  $p(\boldsymbol{\theta}, \sigma_y^2 | \cdot)$ .
-

## 2 Computational speedups from input scaling

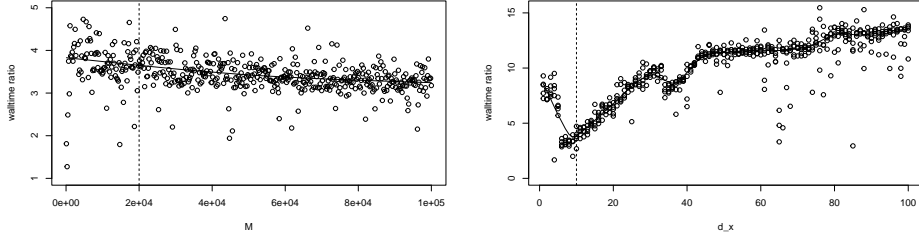
A simple simulation study is presented to show the kind of computation gains that can be expected by the use of input scaling. In the manuscript, two important benefits of input scaling are discussed; First, by scaling inputs, nearest neighbor subsets are dramatically improved when using an isotropic correlation function. This allows us to bypass the expensive step of computing optimal neighborhoods with laGP. By default laGP uses the ALC criterion to do this, which we will explore in this study. Second, scaling inputs allows us to estimate the lengthscales only once, rather than at every prediction. For sequential prediction this can be a very important reduction in computational cost as we will see. The simulation study indicates that speedups due to input scaling could be as large as 2 orders of magnitude (100x) when using the default ALC criterion with parameter estimation compared to nearest neighbors with pre-estimated lengthscales.

### 2.1 Neighborhood selection with laGP

The goal of this study is to quantify the relative cost of the ALC criterion over a range of data set sizes. First, we fix the dimension of the input space at  $d_x = 10$  and generate 500 random datasets with  $100 \leq M \leq 100000$ . Input and output data  $\mathbf{X}$ ,  $\mathbf{y}$  are generated uniformly on the unit hypercube. Predictions are made sequentially at 10 locations using both the ALC and NN criteria. Input scaling is not used, so correlation parameters must be estimated for each prediction. Additionally, 500 datasets are generated with fixed  $M = 20,000$  and  $1 \leq d_x \leq 100$  with 5 repeated datasets generated for each value of  $d_x$ . We see that ALC is between 3 and 5 times slower than NN over a large range of  $M$  at  $d_x = 10$  and increases for larger  $d_x$ . There is significantly more variability in the ratio as we change  $d_x$  while keeping  $M$  fixed, with ratios ranging from 3 to 15. Vertical black lines in Figure 1 are representative of the application data set size ( $M = 20000, d_x = 10$ ).

### 2.2 Parameter Estimation with laGP

The other benefit to input scaling is fixing the correlation parameters for prediction. The cost of repeated parameter estimation during prediction, even



(a) Ratio as a function of ensemble size ( $M$ ). (b) Ratio as a function of input dimension ( $d_x$ ).

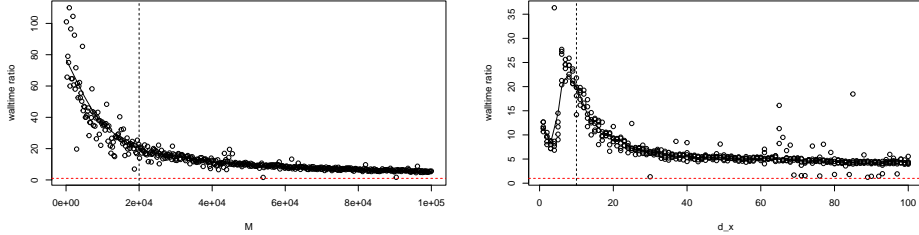
Figure 1: Comparison of wall time for ALC neighborhood selection compared to simple nearest neighbors. For fixed  $d_x$ , ratio decreases slightly with increasing  $M$ , and for fixed  $M$  ratio increases with increasing  $d_x$  after about  $d_x = 5$ . Vertical black lines indicate the approximate size of the application dataset.

for small  $m$ , can add up to be significant over thousands of MCMC iterations. A similar simulation study is performed comparing prediction time for the NN criteria with local parameter estimation, and the NN criteria assuming that global lengthscales have been pre-estimated, and the results are shown in Figure 2. As both  $M$  and  $d_x$  increase, the ratio appears to be converging to 1 (horizontal red line). This is because the computation time associated with finding nearest neighbors dominates that of parameter estimation for large data. For  $M = 20,000$  and  $d_x = 10$  (vertical black lines), which approximately represents the application dataset, speedups are still very significant at (about  $20\times$ ). Assuming a  $5\times$  speedup from NN vs ALC, and a  $20\times$  speedup from pre-estimated lengthscales, we have approximately a 2 order of magnitude speed increase. Obviously, the time required to pre-estimate the lengthscales should not be ignored, but even for the large application dataset considered the cost of pre-estimation is very small compared to the cost of sequential prediction in during Bayesian calibration.

### 3 Computational comparison to sVecchia

The scaled Vecchia approximation (?) is similar to the proposed approach in that it uses input scaling and a subset of the computer model runs for parameter estimation and prediction. The sVecchia model could easily be adapted





(a) Ratio as a function of ensemble size ( $M$ ). (b) Ratio as a function of input dimension ( $d_x$ ).

Figure 2: Comparison of computation time for nearest neighbor selection with and without repeated parameter estimation.

for use in a modular calibration framework. However, we have found that the overhead associated with the Vecchia approximation in the emulator fitting step is significant. Using a modified ball drop example from Section 3.2, we present a comparison of the proposed FlaGP framework with sVecchia to demonstrate this. The size of the data used are representative of the application dataset with  $M = 20,402$ ,  $d_x = 10$ , and  $d_y = 1,500$ . The same 2 relevant inputs are used, Radius and Coefficient of drag, and 8 noise inputs are added. The available sVecchia implementation does not innately handle functional response, so we manually fit independent models in parallel to 2 basis functions. We also make a small adjustment to the sVecchia code to allow for model fitting with a predefined set of inputs, rather than random sampling. These inputs are chosen by FlaGP using stratified random sampling. By using the same subset of inputs for model fitting, results are more comparable. We also choose the same fixed nugget of  $10^{-7}$  for fitting both models. Some variables cannot be made equal in the comparison. Importantly, sVecchia uses the Matérn 7/2 covariance by default and does not have the option for a Gaussian covariance function. The FlaGP model implementation is currently limited to the Gaussian covariance. Differences in predictive accuracy, albeit small, could be in part due to this difference.

We see that the default sVecchia provides only a marginal increase in predictive accuracy at a significant increase in computation time (more than  $3\times$ ). This is only one dataset, and no tuning of the methods was done, so the results here are not meant to be a rigorous comparison of methods. Column 2, the fit time, in Table 1 is our main concern, as it gives a frame

of reference for the significance of the added computational complexity due to the Vecchia approximation. As with comparisons to the SVDGP model, we do not expect that predictive scores from the FlaGP model will be an improvement on sVecchia. What we care about is that predictions from the FlaGP model are accurate, and that the model can be implemented faster for large datasets.

In our experience with the sVecchia model, we have seen that the effect of tuning can be significant. To see this, we present a small comparison on the piston function. We found that the predictive performance of FlaGP was superior to the default sVecchia with  $\nu = 3.5$ , however sVecchia could be made to beat FlaGP by increasing the smoothness parameter for the Matérn to  $\nu = 11/2$ . The point being that these comparisons suggest that FlaGP can be both faster and provide competitive prediction to sVecchia in many settings, however these methods have many tuning parameters and a fair comparison between them is not straightforward. Especially for sVecchia, the interplay between its parameters *n.est* and *m* has a dramatic effect on model fit time and neither parameter is directly comparable to the subsample size used for lengthscale estimation in FlaGP.

This comparison also provides a reference for other methods. The sVecchia approach is designed to be extremely fast. Inference uses a fisher scoring technique, which we have found to be faster than other MLE approaches. We found the maximum likelihood based methods implemented in the R package `mlegp`, which are limited by the same scaling as SVDGP, is infeasible for these data. The NNGP might be feasible, but will naturally be limited due to MCMC in the model fitting step.

Model	Fit time (s)	Pred time (s)	RMSE	MAPE
FlaGP	14.453	0.865	0.0019	0.4458
sVecchia	53.414	0.715	0.0016	0.4145

Table 1: Comparison of FlaGP and sVecchia on the a modified ball drop example with an ensemble size of 20,000.

Model	Fit time (s)	RMSE
FlaGP n.est=400	7.544	0.00072
sVecchia n.est=400 m=400 nu=3.5	23.581	0.00373
sVecchia n.est=2000 m=30 nu=3.5	5.263	0.00367
sVecchia n.est=1000 m=30 nu=5.5	18.803	0.00034

Table 2: Comparison of FlaGP and sVecchia on the Piston function with an ensemble of size 10082. Predictions are compared on an out of sample test set of size 1058. The tuning parameters and correlation functions in sVecchia make a direct comparison to FlaGP difficult.

## 4 AI-5083 Small Ensemble Comparison

### 4.1 Emulation

In the manuscript, we analyze a large ensemble of 20000 runs from the FLAG simulator. A smaller ensemble of size 1000 was previously analyzed in ?. Other than the ensemble size, a major difference between these data and those analyzed in the manuscript is that only 4 points (or features) from each velocity profile are used as the functional response for emulation and calibration. An example curve with the features highlighted is shown in Figure 3. Here we present an analysis of these data using the proposed framework, and give a comparison to ?.

Following the spirit of the emulator validation results presented in ?, a similar leave-one-out cross validation study of the emulator over the design points is presented here. Fig. 4 shows median absolute percent error (MAPE) of predictions over the 12 features of interest from the 3 shots as well as the overall MAPE for all features. Features 2 and 4 are very well predicted for all shots. Both FlaGP and SVDGP give MAPE < 1% for nearly all combinations of subsample and neighborhood sizes. SVDGP is only a marginal improvement over FlaGP for these features. Features 1 and 3 are more difficult to emulate. Even so, FlaGP is within 1.3% performance of SVDGP using a subsample size of 500 for lengthscale estimation and a neighborhood size of 250 for prediction. For all features combined, SVDGP has a MAPE of 1.7% and FlaGP has a MAPE of 2.3%. We believe this performance is very competitive given the computational savings.

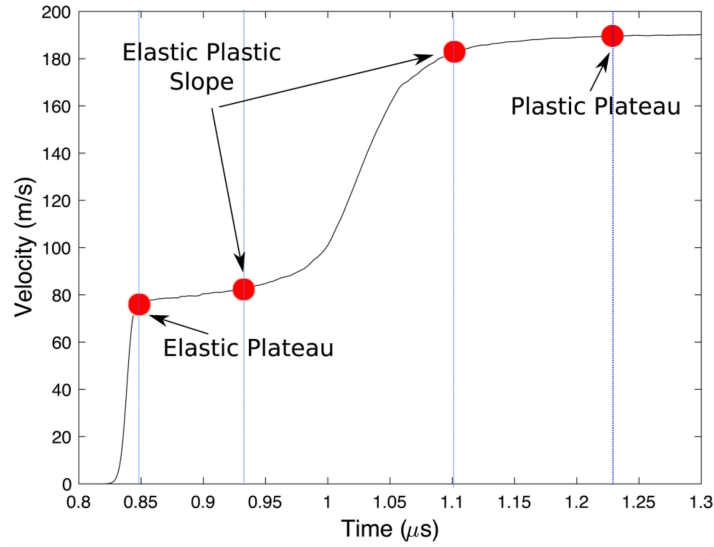


Figure 3: Representative velocity profile with 4 features of interest highlighted.

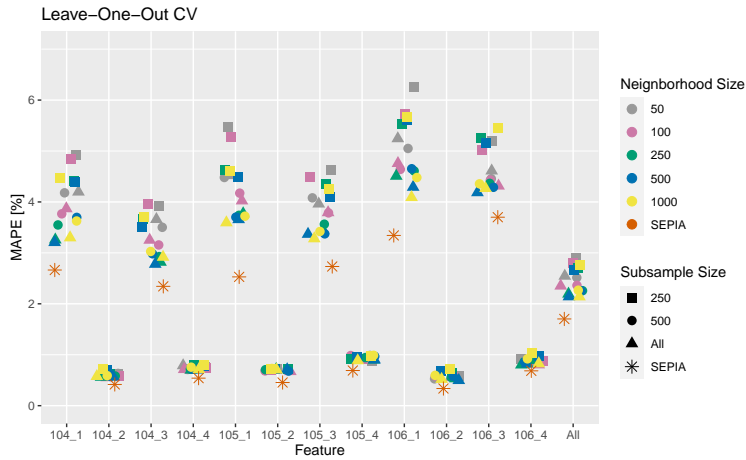


Figure 4: Leave-one-out CV prediction MAPE over a number of subsample and neighborhood sizes. SVDGP results are given for comparison.

## 4.2 Calibration

Constraining the FLAG input parameters using observation is a principal motivation of this analysis. While ? do not discuss computation time asso-

ciated with their MCMC calibration, it is possible to make a rough estimate using the SEPIA code. We found that MCMC using the SVDGP model takes approximately 5 seconds per iteration, meaning the 175,000 posterior samples collected may have taken over 10 days. On the other hand, by setting  $m_c = 50$ , where  $m_c$  denotes the neighborhood size used for calibration, the proposed method allows for 100000 samples to be collected in just 13.5 minutes. Fig. 4 shows that emulation generally improves with increasing  $m$ . For calibration, increasing  $m_c$  seems to be less impactful. Fig. 5 shows posterior density estimates from 75,000 post burn-in posterior samples using  $m_c = 50$  and  $m_c = 250$  as blue and red lines. Posterior density estimates are quite similar, but with  $m_c = 250$ , 100000 samples took 2 hours to generate.

For this calibration, a Half-Cauchy prior is used for  $\sigma_y^2$  with a scale parameter of  $1/2$ . The Half-Cauchy is used because it was found that inference on  $\sigma_y^2$  is sensitive to the choice of Inverse Gamma prior. The Half-Cauchy is generally smoother and the scale parameter of  $1/2$  is selected because it gives some increased weight to small values but is not sharply peaked near 0 and we have found that inference is not very sensitive to this scale parameter. For example, a more sharply peaked Half-Cauchy with a scale of  $1/4$  and a flatter Half-Cauchy with a scale of 1 give similar inferences for  $\sigma_y^2$ . This insensitivity to prior distribution is desirable because we do not have strong prior information about  $\sigma_y^2$ .

The model is able to constrain  $A$  well, and can also constrain flyer plate velocities fairly well. Posterior densities for  $B, C, n_{JC}, m_{JC}, \Delta_2$  are very near to their uniform prior distributions. Fig. 8 in ? show different posteriors with smaller variance. Since we cannot speak to the truth behind the posterior distributions, the quality of calibration is assessed by the models ability to reproduce the field observations. The proposed method allows for a different choice of neighborhood size for calibration and prediction. For both sets of samples different neighborhood sizes for prediction were explored and no gain was found for  $m > 50$ . We also present results for FlaGP models using the MAP approach from Section ???. For these data, the MAP approach outperforms the MCMC approach, but we consider its lack of parameter uncertainty to be a major drawback.

In Fig. 6 predictive means and 95% intervals for predictions using  $m = 50$  are shown. There are small differences in mean predictions for  $m_c = 50$  and  $m_c = 250$  along with a slight reduction in uncertainty when using a larger neighborhood. Predictions are generally very good, with feature 106<sub>1</sub> being the most challenging prediction for FlaGP, but the true value is still

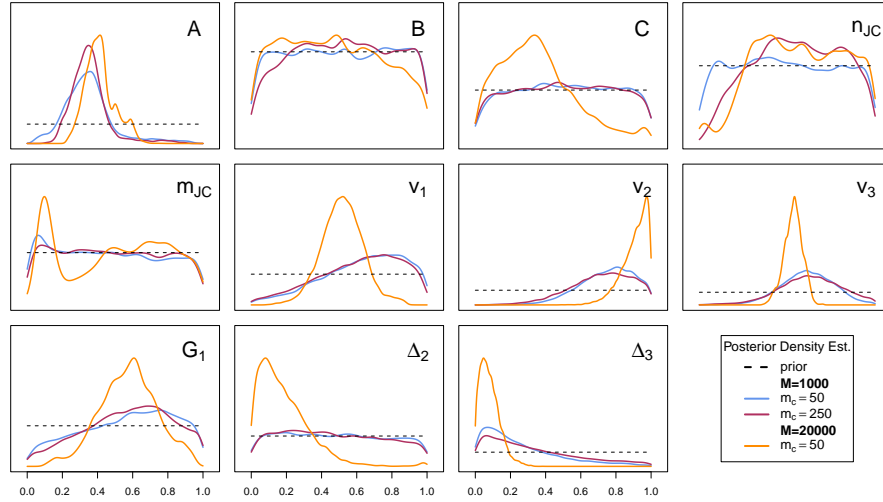


Figure 5: Posterior density estimates from 75000 samples for both ensembles with  $m_c \in \{50, 250\}$ .

captured by the 95% intervals. While this is only one dataset, these results give further evidence to the viability of the FlaGP emulator. Not only is it competitive with the expensive SVDGP approach, it may be preferable for large ensembles due to the fast nature of the algorithm. An MCMC analysis of these data is performed in a moderate amount of time on a personal laptop, while SVDGP takes days on a powerful supercomputer.

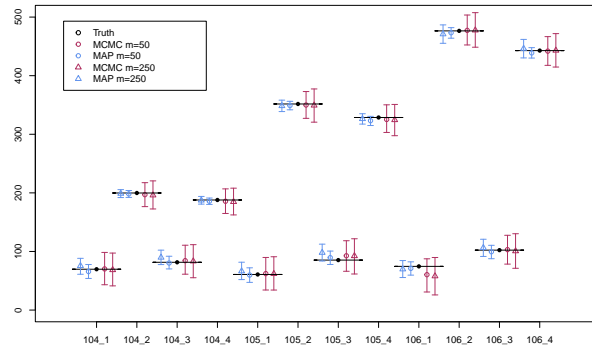


Figure 6: Posterior predictive means and intervals for the observed data are given using calibrated emulators with  $m_c \in \{50, 250\}$ , and  $m = 50$ .